Large-scale ice clouds in the GFDL SKYHI general circulation model

Leo J. Donner, Charles J. Seman, Brian J. Soden, Richard S. Hemler, and James C. Warren

NOAA Geophysical Fluid Dynamics Laboratory, Princeton University, Princeton, New Jersey

Johan Ström

International Meteorological Institute, University of Stockholm

Kuo-Nan Liou

Department of Meteorology, University of Utah, Salt Lake City

Abstract. Ice clouds associated with large-scale atmospheric processes are studied using the SKYHI general circulation model (GCM) and parameterizations for their microphysical and radiative properties. The ice source is deposition from vapor, and the ice sinks are gravitational settling and sublimation. Effective particle sizes for ice distributions are related empirically to temperature. Radiative properties are evaluated as functions of ice path and effective size using approximations to detailed radiative-transfer solutions (Mie theory and geometric ray tracing). The distributions of atmospheric ice and their impact on climate and climate sensitivity are evaluated by integrating the SKYHI GCM (developed at the Geophysical Fluid Dynamics Laboratory) for six model months. Most of the major climatological cirrus regions revealed by satellite observations appear in the GCM. The radiative forcing associated with ice clouds acts to warm the Earth-atmosphere system. Relative to a SKYHI integration without these clouds, zonally averaged temperatures are warmer in the upper tropical troposphere with ice clouds. The presence of ice produced small net changes in the sensitivity of SKYHI climate to radiative perturbations, but this represents an intricate balance among changes in clear-, cloud-, solar-, and longwave-sensitivity components. Deficiencies in the representation of ice clouds are identified as results of biases in the large-scale GCM fields which drive the parameterization and neglect of subgrid variations in these fields, as well as parameterization simplifications of complex microphysical and radiative processes.

1. Introduction

Studies with general circulation models (GCMs) have suggested that atmospheric ice may play an important role as a climate regulator. *Ramanathan et al.* [1983] showed that basic characteristics of a GCM climate can depend strongly on the radiative properties of ice clouds. Numerous studies, including *Wetherald and Manabe* [1988], *Mitchell et al.* [1989], and *Senior and Mitchell* [1993], have shown that climate sensitivity, for example, to radiative perturbations from trace gases, depends on atmospheric ice. Ice-cloud formation, maintenance, and dissipation are products of complex microphysical and dynamical processes, and the role of ice clouds in climate is a balance between the competing tendencies of the clouds to cool through their effect on solar radiation and to warm through their effect on terrestrial radiation.

A useful distinction in GCM studies of ice clouds is in terms of their direct formation mechanism, i.e., convection versus large-scale ascent. In reality, many ice clouds represent mixtures or are results of other processes, but even in ground-based and satellite observations, this distinction can be made.

The properties and roles of convective and large-scale cirrus are likely to differ greatly. Convective cirrus are often optically and geometrically thick and have recently been the focus of intense study regarding their role in the climate system through feedbacks involving solar radiation [e.g., *Ramanathan and Collins*, 1991; *Wallace*, 1992]. *Randall et al.* [1989] documented interactions between these clouds and radiative and hydrological processes. Large-scale cirrus are generally thinner, lacking the water source provided by convection, but occur with much greater frequency than convective cirrus. Their ice contents vary over a range resulting in emissivity variations to which the general circulation may be quite sensitive [*Ramanathan et al.*, 1983; *Lohmann and Roeckner*, 1995]. A measure of the relative frequency of convective cirrus is provided by the conditional probability of cumulonimbus clouds, given the presence of cirrus. This probability ranges from 4 to 20% in the tropics, depending on season and whether the surface is land or ocean [*Warren et al.*, 1985]. (Of course, some detached cirrus may have originated convectively, demonstrating the limitations of this simple decomposition.) GCM parameterization strategies for large-scale and convective ice clouds emphasize treatment of large-scale dynamics and cumulus parameterization, respectively, although the two parameterizations ultimately interact.

The purpose of this paper is to study large-scale ice clouds in a GCM: their distribution, microphysical and radiative prop-

erties, and impact on climate and climate sensitivity. A simple, process-based parameterization will be employed in the Geophysical Fluid Dynamics Laboratory (GFDL) SKYHI GCM. Sections 2 and 3 describe the microphysical and radiative properties of the modeled ice clouds and the procedures used in their calculation. Section 4 presents key results on the effect of the ice clouds on SKYHI's thermodynamics, dynamics, and hydrology. Section 5 indicates the effect of atmospheric ice on climate sensitivity.

2. Parameterizations of Microphysical and Radiative Properties of Large-Scale Ice Clouds

The parameterization for large-scale ice clouds is based on *Heymsfield and Donner* [1990]. In this parameterization, two classes of large-scale ice clouds are treated. Saturated ice clouds form when large-scale ascent occurs in sufficiently cold, moist layers. Sublimating clouds form in drier layers below saturated ice clouds. Equilibrium solutions for ice content are obtained by solving prognostic equations for the saturated clouds; in the prognostic equation, ice is formed by deposition from vapor to ice and removed by gravitational settling. The ice content in sublimating clouds depends on humidity and temperature and is an approximation of detailed microphysical calculations. Some extensions and simplifications of *Heymsfield and Donner* [1990] have been incorporated to facilitate GCM implementation.

2.1. Ice Cloud Thickness

The vertical resolution of GCMs in the middle and upper troposphere is fairly coarse, and the vertical extent of ice clouds can be considerably less than the thickness of GCM layers. For example, *Starr and Wylie* [1990] observed in a First ISCCP (International Satellite Cloud Climatology Project) Regional Experiment (FIRE) case that cirrus generation was typically restricted to layers of about 0.5 km depth. By contrast, SKYHI's resolution is around 1 to 1.5 km in the middle and upper troposphere. A parameterization which allows for the possibility of vertically subgrid clouds is desirable. *Heymsfield and Donner* [1990] parameterized only ice content; however, their procedure implies a cloud thickness. They considered the ice content of a thin layer undergoing lifting within the interior of an ice cloud. Deposition from vapor to ice occurs in this layer, increasing its ice content as it is lifted. The temperature gradient across this layer results in different rates of ice accumulation at its top and bottom. Fluxes of ice due to gravitational settling, F, remove ice from the layer during its lifting, where

$$F = X_s \rho V_t. \tag{1}$$

Here X_s denotes the ice mass mixing ratio; ρ is the air density; and V_t is the mean terminal speed of the ice-particle distribution. The terminal speed is parameterized as a function of ρ and X_s, as in the *Heymsfield and Donner* [1990] work. Since X_s varies vertically across the layer as a consequence of the temperature gradient across the layer, there exists a local divergence of the ice flux (dF/dz). This ice-flux divergence determines the rate at which ice is removed from the thin layer as it is lifted. As discussed by *Heymsfield and Donner* [1990], the parameterized ice content is the average ice content in the layer and results from an equilibrium between the rates of

depositional accumulation of ice and ice removal by gravitational settling. If this ice content is applied to a cloud of finite thickness, then for consistency, the local ice-flux divergence should also apply, on average, over the finite thickness of the cloud. Since the top of the cloud is defined as the level above which the ice content vanishes, there is no downward ice flux there. If the average ice content is then applied to the full cloud thickness, the downward flux at the bottom of the cloud is given by (1), using vertically averaged quantities on the right-hand side. A vertically averaged ice removal ($g\bar{F}/\Delta p$) is implied. The cloud pressure thickness is Δp, g is the gravity constant, and an overbar indicates an average over the full vertical extent of the cloud. If the ice removal rate for the thin layer considered by *Heymsfield and Donner* [1990] is equal to the vertically averaged removal rate over the entire cloud, then Δp is determined:

$$\Delta p = -g\bar{F}\bar{\rho}\left(\frac{dF}{dz}\right)^{-1}. \tag{2}$$

For a physical interpretation of (2), note that timescales and vertical scales for the cloud are related, since the ice removal (sedimentation) rate is proportional to the ice-flux divergence. Using the hydrostatic relationship, substituting dX_s/dt for $1/\bar{\rho}(dF/dz)$, and replacing $\bar{F}$ using (1), the cloud (geometric) thickness is the ratio of $X_s V_t$ to dX_s/dt. The ratio of ice concentration to sedimentation rate provides a timescale for ice removal. The cloud thickness is the product of this timescale and the terminal speed of the crystals; that is, the cloud thickness is the distance that ice crystals fall at their terminal speed over the time when ice is removed by sedimentation.

The numerical procedure for determining X_s and Δp in saturated ice clouds is to use a table constructed following *Heymsfield and Donner* [1990]. The parameters which control saturated ice content and cloud thickness are temperature, vertical velocity, lapse rate, and pressure (given that saturation exists). As in Table 1 in the work of *Heymsfield and Donner* [1990], the ice-flux divergence (dF/dz) is obtained by solving for the ice concentration at two levels, using (1) for F at both levels, and differencing.

2.2. Sublimation in Unsaturated Layers

Heymsfield and Donner [1990] discussed sublimation in unsaturated layers. A variation of their procedure is employed.

A sublimating-ice layer exists in an unsaturated GCM layer which lies immediately below a layer containing ice. If ice-saturated clouds occupy adjacent GCM layers, the sublimating ice forms only below the lowest boundary of the ice-saturated clouds. (This is done even for cases in which the ice cloud thickness in one or more of the adjacent layers is less than the thickness of that layer.) The atmospheric properties below the lower boundary of the ice-saturated cloud and the ice content in the saturated cloud are used to calculate the maximum ice-crystal survival distance, following *Heymsfield and Donner* [1990]. If the maximum ice-crystal survival distance exceeds the distance to the next lowest GCM layer, the ice content at the top of the next lowest layer is calculated by assuming that the sublimating-ice content decreases quadratically in the ratio of the distance below the base of the upper cloud to the maximum ice-crystal survival distance. This procedure is repeated successively downward until the maximum ice-crystal survival distance is less than the thickness of the GCM layer.

Zonally Averaged Cirrus Fraction
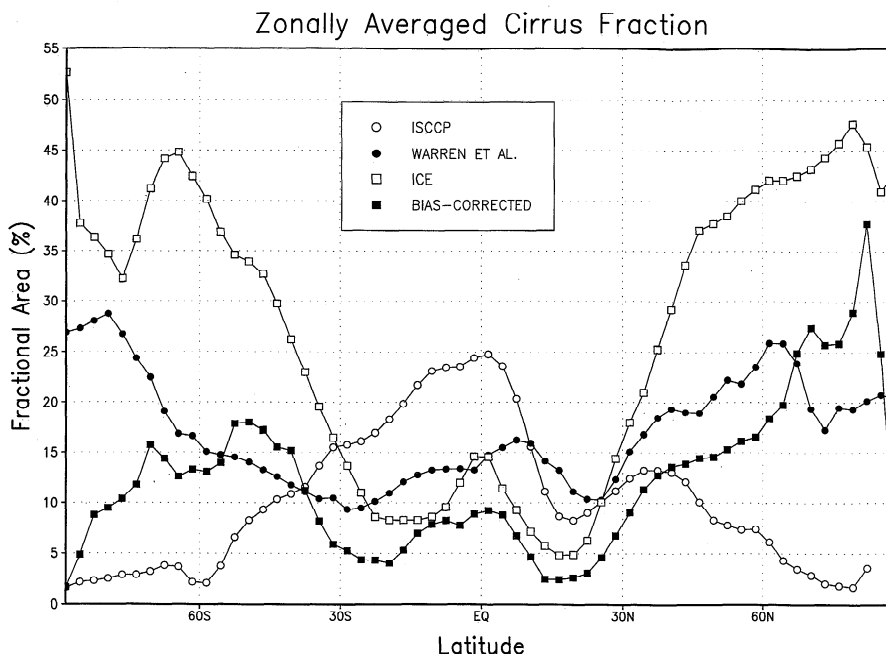
Figure 1. Zonally averaged fractions for large-scale ice clouds (SKYHI) and nonconvective cirrus (satellite and ground observations). Time means for January, February, and March.

2.3. Links to GCM Thermodynamics and Hydrology

The parameterization described above calculates the ice content at each time step in the GCM integration. Changes in ice content must be accompanied by consistent changes in water vapor. The implied phase changes force the large-scale flow through the large-scale thermodynamic equation. In saturated layers, changes in the ice mass mixing ratio are accounted for directly by compensating local changes in the water-vapor mixing ratio X_v:

$$\frac{\partial X_v}{\partial t} = -\frac{\partial X_s}{\partial t}. \tag{3}$$

The ice which sublimates below the ice-saturated layers is supplied from water vapor which is deposited to ice in the saturated layer. For simplicity this water vapor is removed from the lowest layer for multiple-layer ice-saturated clouds:

$$\frac{\partial X_v(p_{sat})}{\partial t} = \frac{1}{\Delta p_{sat}} \int_{p_{sub}}^{p_{sat}} \frac{\partial X_s}{\partial t} H\left(\frac{\partial X_s}{\partial t}\right) dp, \tag{4}$$

where p_{sat} indicates the pressure in the bottom layer of an ice-saturated cloud, p_{sub} is the pressure at the base of a sublimating ice cloud, and Δp_{sat} is the pressure thickness of the lowest ice-saturated layer. The step function H is unity when its argument is positive and zero when its argument is negative.

When the ice content decreases across a time step in a sublimating layer, the decrement is converted into water vapor:

$$\frac{\partial X_v}{\partial t} = -\frac{\partial X_s}{\partial t} H\left(-\frac{\partial X_s}{\partial t}\right) \tag{5}$$

If multiple, separated ice-saturated clouds develop, the sublimating cloud from an ice-saturated cloud above a lower ice-saturated cloud is terminated at the top of the lower ice-saturated cloud. Any sublimating flux which reaches the ground becomes surface precipitation. (Note from *Heymsfield*

and Donner [1990] that sublimating ice may melt and subsequently evaporate if the layers below the ice-saturated cloud are sufficiently warm.) Taken together, the processes summarized here conserve the sum of condensed water and water vapor and provide for vertical redistribution of water vapor as ice crystals settle and sublimate at lower heights.

The phase changes described above imply corresponding thermodynamic effects. In cases where water vapor is removed, latent heat is released. In layers where condensed water is converted to water vapor, cooling occurs.

2.4. Radiative Transfer in Ice Clouds

Parameterizations of the transfer of shortwave and longwave radiation in ice clouds use the broadband approach described by *Liou et al.* [1991]. The broadband longwave emissivity and shortwave reflectance (albedo) and absorptance are parameterized in terms of ice water path and the mean effective size of the ice-particle distribution. For solar radiation, a zenith angle of 60° is used. The broadband approach for determining ice-cloud radiative properties is consistent with the overall radiative-transfer framework in SKYHI [*Fels et al.*, 1980].

The broadband ice-cloud radiative parameters are determined from the single-scattering properties for ice-crystal size distributions which are driven by temperature, as described subsequently. The shortwave and longwave spectra are divided into six and 12 bands to resolve the variation in the refractive index of ice and to account for the gaseous absorption, principally by water vapor. The delta-four-stream method is used to compute the broadband radiative properties in a manner described by *Liou et al.* [1991]. The scattering and absorption properties of hexagonal ice crystals assuming columns and plates are calculated from the geometric ray-tracing technique for size parameters larger than 30. For smaller-size parameters, we use the Mie-type solution for spheroids to approximate the single-scattering properties for ice particles. Small-size parameters generally occur in the longwave in which ice has

(a) "Ice" Experiment Ice-Water Path [g/(m**2)]

(b) "Bias-Corrected" Experiment Ice-Water Path [g/(m**2)]
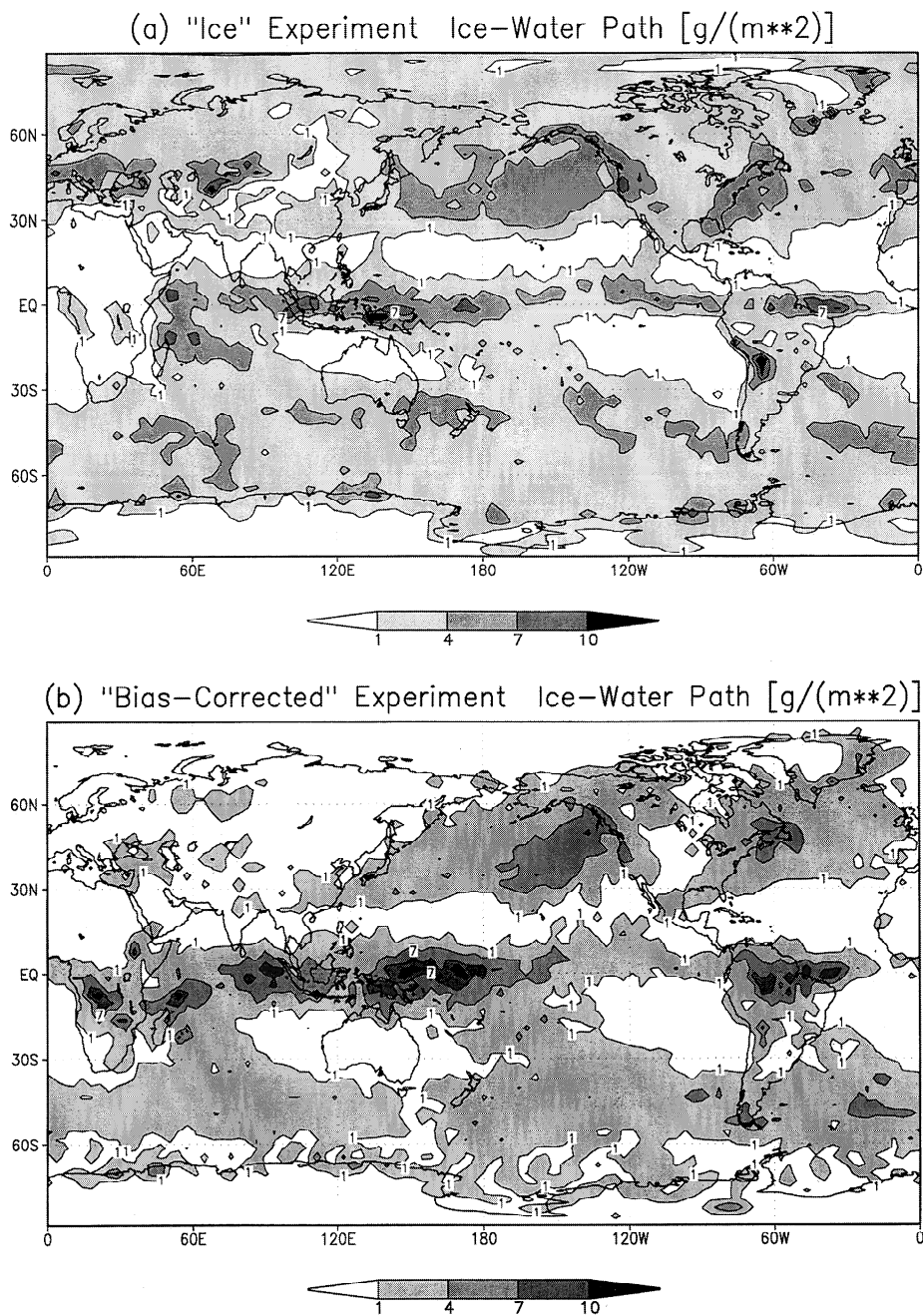
Figure 2. Mean ice-water path for (a) "ice" and (b) "bias-corrected" integrations; (c) conditional (on cloud occurrence) zonally averaged ice paths for Figures 2a and 2b.

strong absorption. For this reason, it appears that ice-crystal shape effects would become less significant.

To allow the dependence of solar albedo on zenith angle, the parameterization equation developed by *Ramanathan et al.* [1983] for the solar albedo *a* is followed, in the form

$$a = \frac{C_i}{C_i + \zeta},$$ (6)

where ζ is the cosine of the zenith angle. C_i is determined by using the values of a at $\zeta = 0.5$ in accordance with the preceding parameterizations. In doing so, the values for C_i become dependent on the microphysical properties in terms of ice water path and particle size generated in the model.

It is immensely difficult to estimate the mean particle size

for ice distributions but important to do so, given its large role in determining radiative properties. From the perspective of radiation calculations, particles scatter light in proportion to their cross-sectional area, which in the case of a nonspherical particle is proportional to the maximum dimension multiplied by the width. Following *Liou et al.* [1991], the mean effective size D_e for a distribution of ice particles is defined by

$$D_e = \frac{\int_{L_{min}}^{L_{max}} D^2 Ln(L)\ dL}{\int_{L_{min}}^{L_{max}} DLn(L)\ dL},$$ (7)

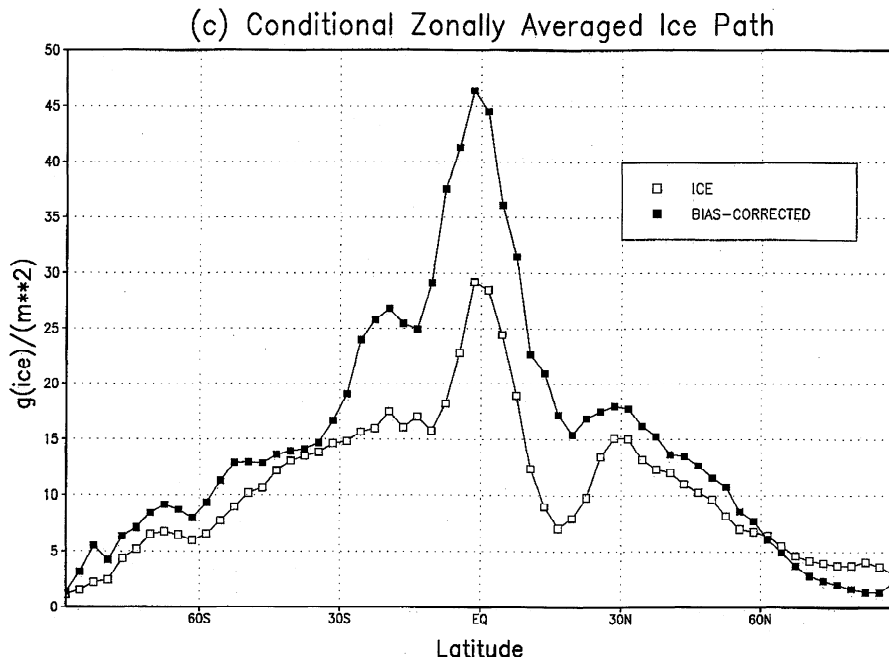## (c) Conditional Zonally Averaged Ice Path

Figure 2. (continued)

where L and D denote the ice-crystal maximum and minimum dimensions, respectively. The terms L_{min} and L_{max} are the maximum and minimum values for L, and $n(L)$ is the ice-crystal size distribution. On the basis of the observations presented by *Heymsfield and Platt* [1984], $n(L)$ is a function of ice-water content and temperature. The functional relationship between D and L can also be determined from observations. It follows that (7) is solved as a function of temperature [see also *Ou and Liou*, 1995].

The ice-crystal size distribution function developed by *Heymsfield and Platt* [1984] holds only for ice-crystal sizes with the maximum dimension greater than 20 μm. They estimate that the fraction of the visible extinction coefficient due to ice particles with sizes from 1 to 20 μm as a function of temperature can exceed 50%. For this reason, a correction to the value of D_e to account for the effects of small particles has been developed on the basis of the formulation for visible optical depth presented by *Ebert and Curry* [1992] in the form

$$\tau = \left(\frac{1}{g}\int X_s \, dp\right)\left(\alpha + \frac{\beta}{r_e}\right), \qquad (8)$$
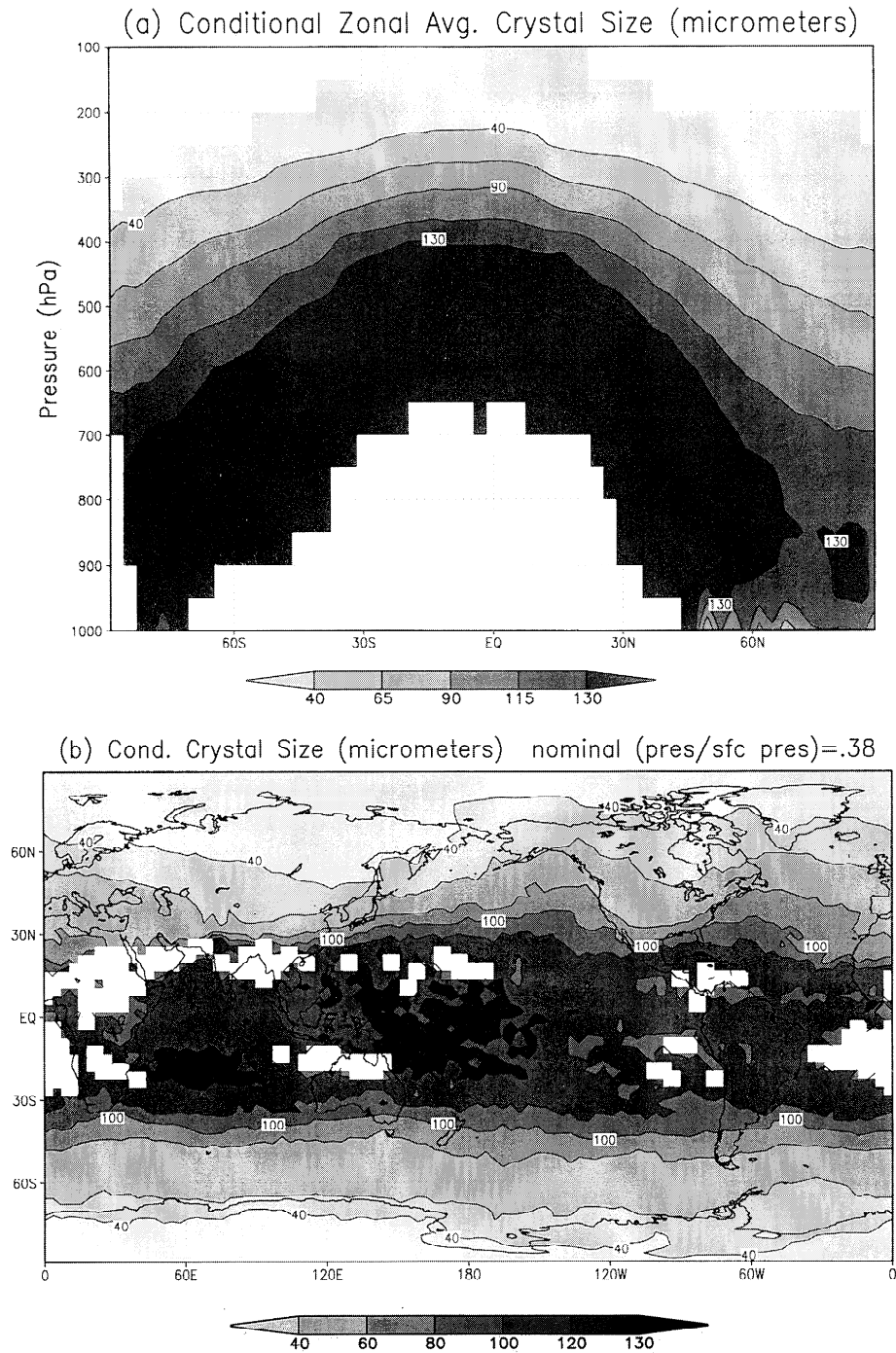
where p denotes pressure, α and β are constants, and r_e is an effective radius. The effective radius is obtained by replacing D and L in (7) with the radius of a sphere whose surface area is the same as the area of the corresponding member of the ice-particle distribution. Using *Heymsfield and Platt*'s [1984] temperature-dependent estimate of the contribution of small particles to the visible extinction coefficient, (8) can be solved for a corrected value of r_e, which increases the optical depth by the appropriate fraction. The corrected values of r_e are converted to corrected values of D_e by equating the surface areas of spheres of radius r_e to areas of hexagonal cylinders whose characteristic dimensions are D and L, consistent with *Liou et al.* [1991] and *Heymsfield and Platt* [1984]. This procedure avoids inverting *Liou et al.*'s [1991] nonanalytic relationships

involving D_e and optical depth while providing ice-crystal sizes consistent with observations.

2.5. SKYHI Implementation and Experiments

The basic characteristics of the SKYHI GCM used in these experiments are as in the work of *Fels et al.* [1980] with a resolution of 3° latitude by 3.6° longitude. The cloud distribution in this version of SKYHI ("control") is prescribed and zonally averaged. This version of SKYHI has 40 vertical levels. Sea surface temperatures are prescribed and vary with season. Radiation has a diurnal cycle. The model employs vertical fourth-order finite differences, important for accurate treatment of advection of water vapor, which is an important control on cloud formation. This version of SKYHI suffers from a cold bias in the upper tropical troposphere, and the prescribed clouds in the "control" version are obviously quite idealized. The impact of SKYHI biases is considered in greater detail later.

Several SKYHI experiments assess the role of ice clouds in the general circulation, demonstrate the effect of the parameterization on SKYHI relative to its "control" version, and examine the effect on parameterized ice of biases in the fields which determine ice cloud properties. For these experiments, "control" prescribed clouds are removed whenever the temperature in SKYHI falls to 258 K, which is the temperature at which *Heymsfield and Donner* [1990] allow saturated ice clouds to form. The large-scale relative humidity at which saturated ice clouds are allowed to exist within a GCM grid cell is 70%; since the ice clouds may not be so thick as the GCM grid cell, large-scale saturation is not necessary. The large-scale ice clouds are assigned a horizontal fractional area of unity; this simplification can lead to an inconsistency between the fraction of the SKYHI grid volume filled with ice and the large-scale relative humidity, since the thicknesses calculated using (2) and the sublimation parameterization do not necessarily satisfy ice-volume constraints posed by the large-scale relative humid-

(a) Conditional Zonal Avg. Crystal Size (micrometers)

(b) Cond. Crystal Size (micrometers) nominal (pres/sfc pres)=.38

Figure 3. Effective crystal sizes, conditionally averaged over cases of ice-cloud occurrence: (a) zonal average; (b) horizontal distribution on model surface whose ratio of pressure to surface pressure is 0.38 for a nominal surface pressure of 1013.25 hPa. Ice clouds do not form in white areas.

ity. The 70% threshold is chosen on the basis that its frequency of occurrence in SKYHI in the regions where large-scale ice clouds are allowed to form is approximately the fractional area of nonconvective ice clouds obtained from ISCCP. SKYHI integrations with this ice implementation are referred to as "ice" integrations. Integrations in which no ice clouds are included (no clouds whatsoever when the temperature is less than or equal to 258 K) are referred to as "no ice" integrations. All experiments were integrated for six model months, starting from an October 1 initial condition extracted from an extended

"control" integration. Results are analyzed from the last three months of the integrations.

As indicated above, ice can form when the relative humidity reaches 70% in the "ice" integrations. Note that additional criteria involving vertical velocity and lapse rate set forth by *Heymsfield and Donner* [1990] must also be satisfied. Saturated ice clouds are not permitted to form at pressures less than 60 hPa or in the model layer closest to the ground. The retention of the prescribed cloud field for temperatures above 258 K provides a distribution of liquid and mixed-phase clouds, which
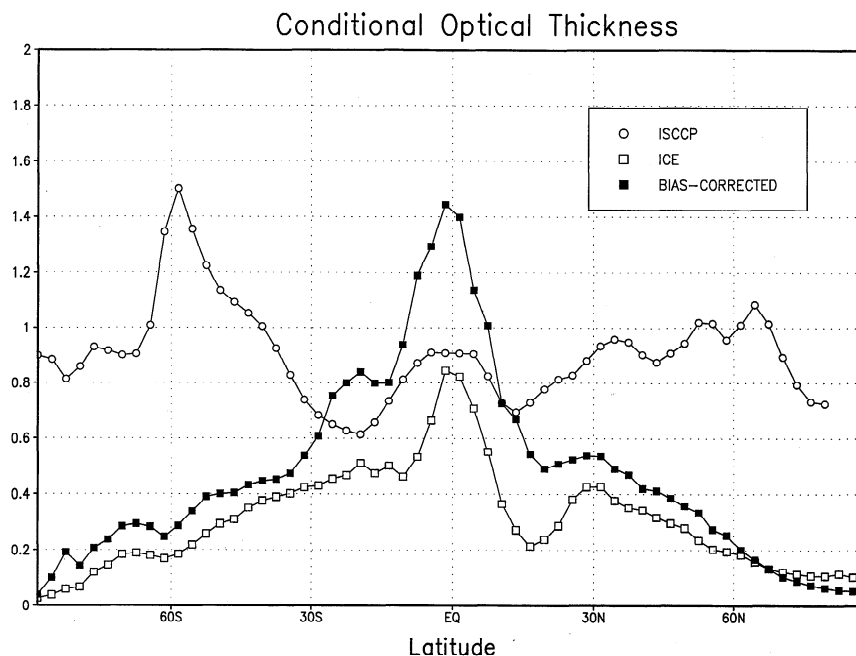
Figure 4. Conditional zonally averaged ice paths for ISCCP and "ice" and "bias-corrected" integrations.

obviously does not interact with the ice clouds, enabling an analysis of their effects isolated from a large set of feedbacks. However, the removal of clouds at and below 258 K, replaced only by large-scale ice clouds, would result in the absence of cirrus associated with deep convection. (The ice parameterization of *Heymsfield and Donner* [1990] does not include basic ice-formation processes associated with deep convection and is not activated when saturated adiabatic adjustment occurs.) Although convective cirrus is not the focus of this study, some representation is required to ensure a reasonable basic cloud distribution about which to study large-scale ice clouds. A parameterization which relates the fractional area of anvil cirrus to the precipitation produced by deep convection [*Slingo*, 1987] is incorporated to do so in the "ice" integration. This precipitation is calculated by the saturated adiabatic adjustment when active between 500 and 100 hPa. The infrared emissivity of anvil cirrus is taken as unity, and the zenith-dependent albedo follows *Ramanathan et al.* [1983].

Hamilton et al. [1995] identified biases relative to observations in SKYHI's temperature field. Biases in temperature as well as those in humidity and vertical velocity will introduce errors in the ice parameterization. A limited assessment of the role of these errors is provided in the "bias-corrected" integration. In these experiments, corrections to temperature, relative humidity, and vertical velocity are applied to these fields for use in the ice parameterization only. The corrections do not vary in time and are means over the last three months of the model integrations. The temperature and vertical-velocity corrections are obtained by differencing European Centre for Medium-Range Weather Forecasts (ECMWF) analyses from SKYHI fields for the "ice" integration. For humidity, *Soden and Bretherton*'s [1993] procedure is used to estimate the upper tropospheric relative humidity. A height-independent correction ratio (relative to the "ice" integration) is applied between 600 and 200 hPa in the "bias-corrected" integration. The temperature correction is applied first, followed by calculation of a corrected relative humidity. The vapor pressure is then cor-

rected by taking the product of the corrected relative humidity and the saturation vapor pressure at the corrected temperature. Thereby, the corrected temperatures and water-vapor mixing ratios are consistent.

Except for "bias corrected," all integrations were started from October 1 in a SKYHI "control" integration and extended six months. Analysis covers January through March. In the "bias-corrected" integration, averaged corrections were obtained for January through March, using 1990 ECMWF analyses. The "bias-corrected" integration was started with initial conditions from the end of the thirteenth week of "ice" and extended through March.

3. Global Distributions of Large-Scale Ice Clouds in SKYHI

As noted in section 2.5, the occurrence of large-scale ice clouds is governed by assumptions regarding large-scale temperature, vertical velocity, relative humidity, and lapse rate. The parameterization of the ice-cloud properties themselves does not address the question of occurrence, but time-mean cloud properties obviously depend on it. Ice cloud properties conditionally averaged on occurrence will be presented in some cases to separate the issue of the microphysical and radiative properties of the clouds from their frequency of occurrence when interpreting time means. Doing so, facilitates comparison of cloud properties with experimental field measurements.

Figure 1 illustrates the zonally averaged fractional areas associated with large-scale ice clouds, formed using the criteria in section 2.5. Also illustrated is an estimate of the nonconvective fractional area for large-scale ice clouds from ISCCP [*Rossow et al.*, 1996]. The ISCCP fractional area is obtained by averaging the cirrus cloud cover (ISCCP cloud-type 13) from all observations in which the deep convective cloud cover (ISCCP cloud-type 15) is less than 1% for that particular grid box. The ISCCP cloud cover is obtained from 3-hourly obser-
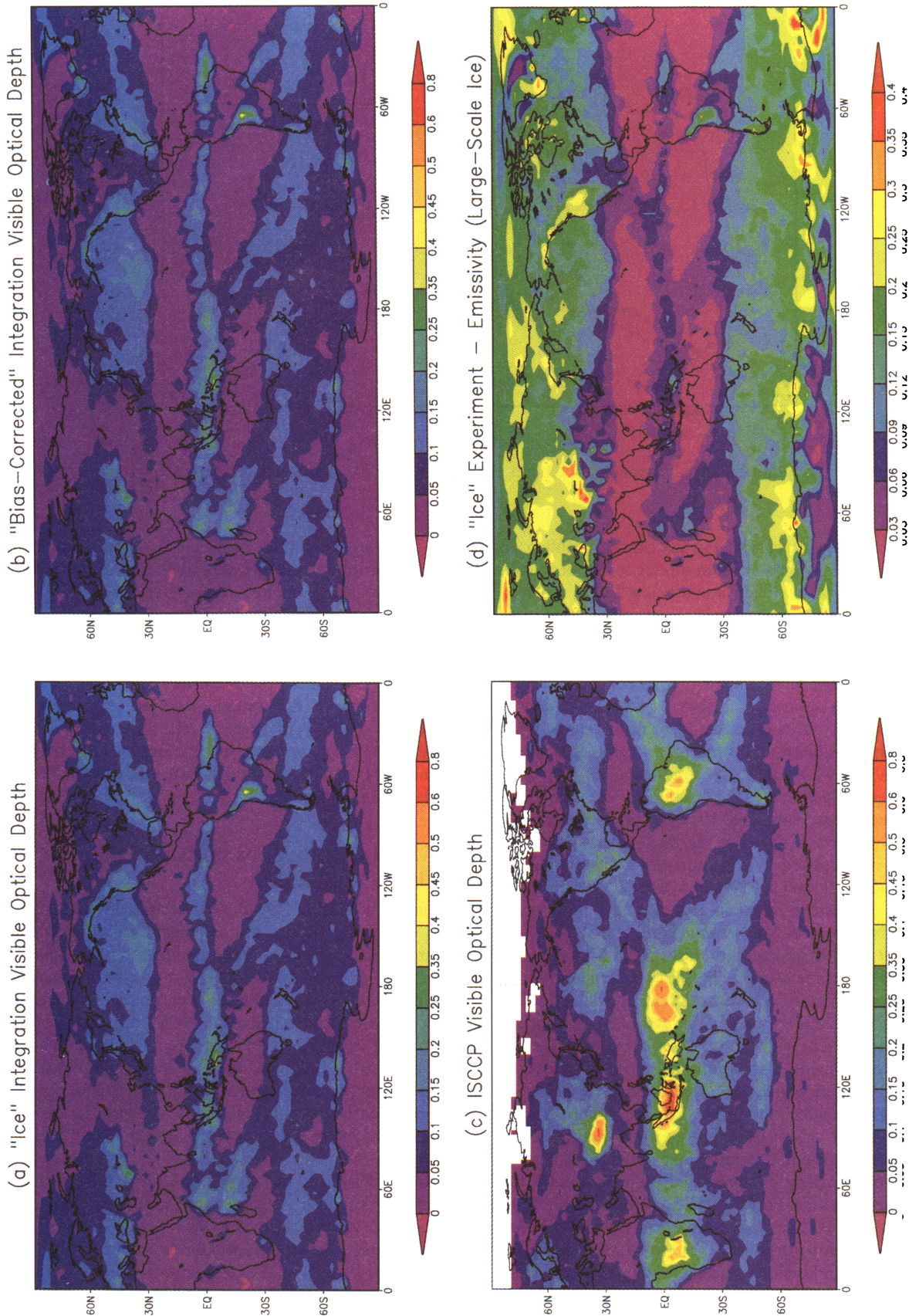
Plate 1. Radiative properties of large-scale ice clouds. Visible optical depths for (a) "ice" integration, (b) "bias-corrected" integration, and (c) International Satellite Cloud Climatology Project (ISCCP) nonconvective cirrus; emissivity for (d) "ice" and (e) "bias-corrected" integrations. Conditionally averaged (on cloud occurrence) visible optical depths for (f) "bias-corrected" integration and (g) ISCCP nonconvective cirrus; (h) conditionally averaged emissivity for "bias-corrected" integration.

(e) "Bias-Corrected" Experiment - Emissivity (Large-Scale Ice)

(f) "Bias-Corrected" Conditional Optical Depth (Large-Scale Ice)
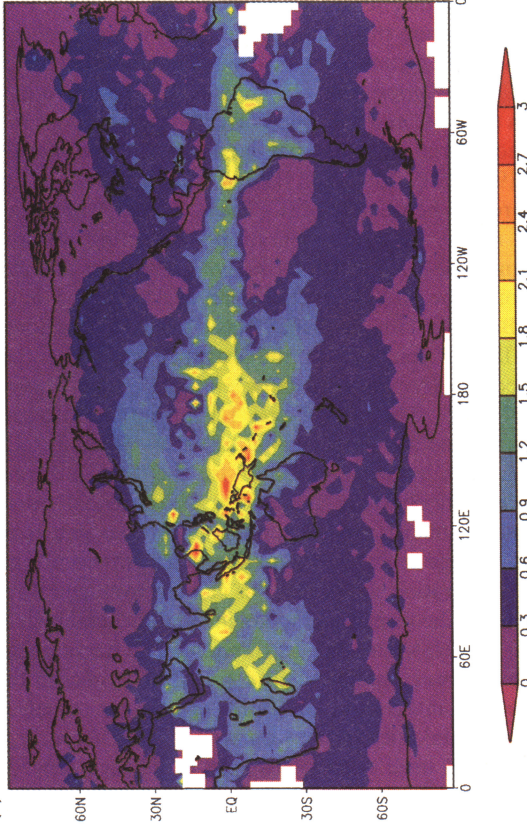
(g) ISCCP Conditional Cirrus Optical Depth
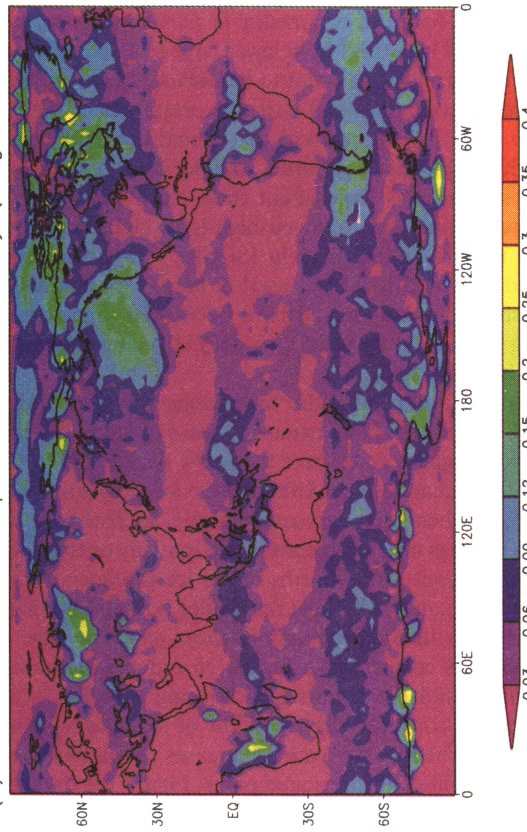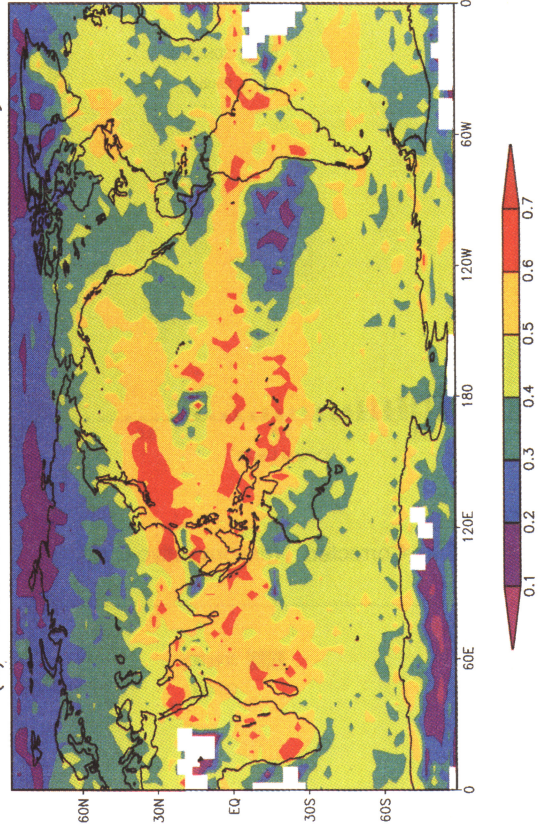
(h) "Bias-Corrected" Conditional Ice Emissivity

Plate 1. (continued)

(a) "Ice" Nonconvective Cirrus

(b) "Bias-Corrected" Nonconvective Cirrus

(c) ISCCP Nonconvective Cirrus
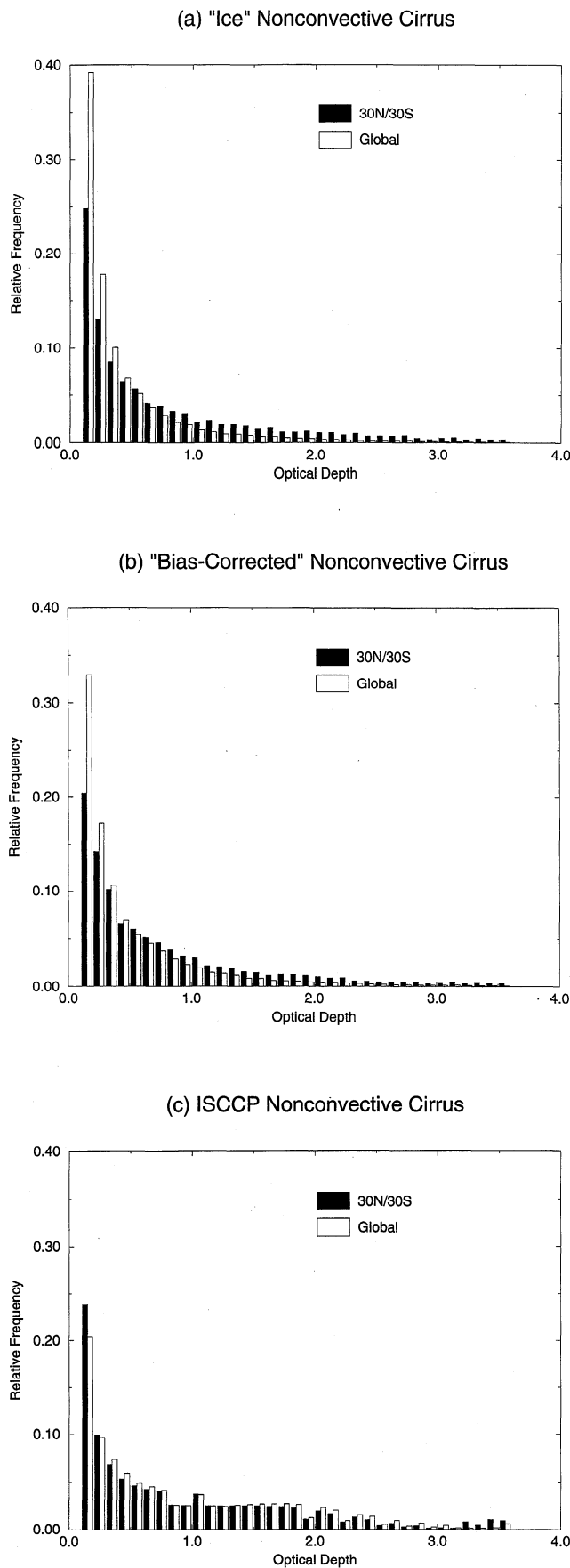

Figure 5. Histograms of visible optical depth for (a) "ice" integration, (b) "bias-corrected" integration, and (c) ISCCP nonconvective cirrus.

vations for January, February, and March 1990. Since visible radiances are required for cloud-type classification, only daytime measurements are used in compiling the ISCCP averages. Also shown are the fractional areas for cirrus, reduced by the fraction when cumulonimbus is simultaneously present, averaged from *Warren et al.* [1984, 1985, 1988] and *Warren* [1986]. Both the "ice" and the "bias-corrected" integrations reproduce the equatorial maximum obtained by ISCCP but not *Warren et al.* [1984, 1985, 1988] and *Warren* [1986]. There are significant differences between the ISCCP and the latter observations, as well as the SKYHI integrations, reflecting differences in ground-based and satellite-observing strategies and cloud definitions. The SKYHI fractions are clearly too low in the tropics. Both the "ice" and the "bias-corrected" fractions exceed the ISCCP fractions in the extratropics, while the "bias-corrected" fractions fall between ISCCP and *Warren et al.* [1984, 1985, 1988] and *Warren* [1986] in the northern middle latitudes and southern high latitudes. As noted in section 2.5, the relative humidity threshold for the "ice" integration was obtained by choosing a humidity whose global tropospheric frequency of occurrence approximately matched that of the ISCCP large-scale ice cloud frequency of occurrence. The "ice" integration shows that this globally averaged threshold is too low in the tropics and too high in middle and high latitudes (with SKYHI's humidity distribution). The fractional area varies less between middle latitudes and the tropics in the "bias-corrected" integration, indicative of a larger negative bias in relative humidities in the tropics in "ice." Of course, relative humidity by itself as an indicator of cloud occurrence is intrinsically limited at spatial resolutions as coarse as those used in these integrations. Tropical "bias-corrected" fractions are lower than those for "ice," despite the application of positive corrections for relative humidity in the ice-cloud parameterization there. This results from lower large-scale relative humidities in "bias-corrected," a point to be discussed later in the context of the microphysical and radiative properties of the clouds.

Jin et al. [1996] reported that climatologies obtained from the high-resolution infrared sounder and the Stratospheric Aerosol and Gas Experiment show more cirrus than ISCCP. (Matched analysis produced high-level cloud amounts about 12% more in HIRS than in ISCCP). If a cirrus climatology based on HIRS had been used in these experiments, a lower threshold humidity would have been used than that selected using ISCCP (section 2.5), so SKYHI cloud amounts would also have increased.

Figure 2a illustrates the time-mean ice-water path for the "ice" integration. Note extensive areas of ice in the intertropical convergence zone, over the north Pacific, 45° to 60°S, and over the Indian Ocean. Although the ice clouds in Figure 2 do not form when deep convection occurs, ice paths are relatively large in areas near deep convection spatially or temporally. On average, about three fourths of the ice is associated with saturated ice clouds, while the remainder is in sublimating clouds, but this partitioning can vary in space and time. The application of bias correction in Figure 2b reduces ice paths in the southern midlatitudes, while producing a region of ice over Africa and consolidating two areas of ice maxima over South America. The bias correction increases ice paths when clouds occur (conditionally averaged paths, Figure 2c) significantly in the tropics. Radiative properties of the clouds depend on both ice path and mean effective crystal size. Figure 3a shows time-mean, zonally averaged crystal sizes, conditional on occurrence of ice clouds. Consistent with the temperature distribution, the

(a) Temperature Diff (K): ECMWF − "Ice" Experiment

(b) Vert Vel Diff (cm/s): ECMWF − "Ice" Experiment
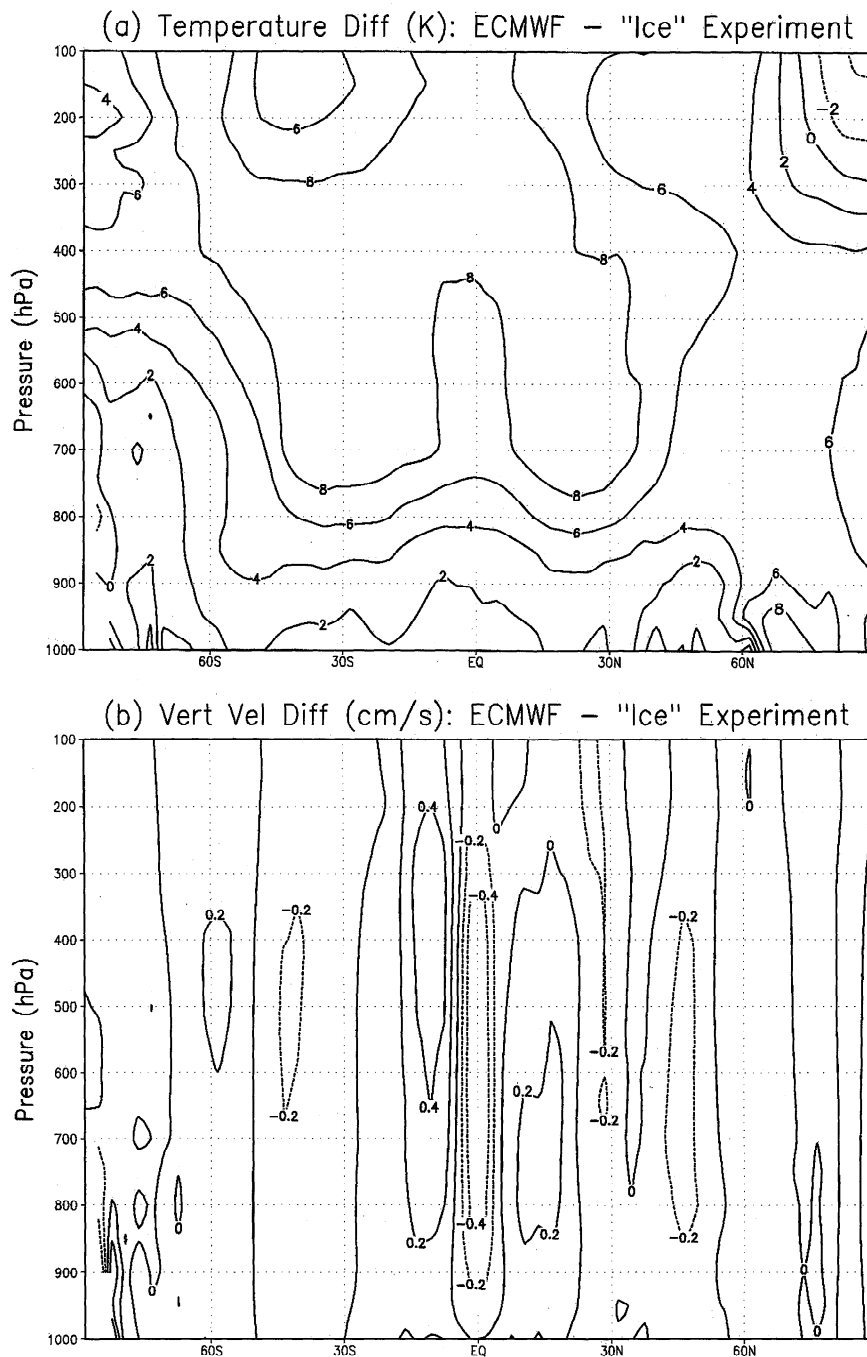
Figure 6. Bias corrections for (a) temperature, (b) vertical velocity, and (c) relative humidity. Zonally averaged corrections are shown for temperature and vertical velocity, but longitudinal variations are also included in "bias-corrected" integration. Dashed lines in Figure 6a denote negative values. The correction factor in Figure 6c is the ratio of satellite-inferred relative humidity to SKYHI's relative humidity.

largest crystals are in lower clouds. Figure 3b shows the distribution of mean effective particle size on a model level where ice clouds frequently occur to provide an indication of horizontal variations. Figures 3a and 3b both suggest substantial variations in mean effective particle size; the consequences for cloud radiative properties are considered later.

The radiative properties of SKYHI's ice clouds are shown in Plate 1. For the "ice" and "bias-corrected" integrations the optical-depth patterns (Plates 1a, 1b) map reasonably well from the ice paths. ISCCP optical depths (averaged temporally

without radiative weighting from 3-hourly observations, to be consistent with SKYHI means) are shown in Plate 1c. The major areas of cirrus activity identified by ISCCP are evident in the SKYHI integrations, especially with bias correction. These include cirrus regions over Africa, the western tropical Pacific, and tropical South America. SKYHI pattern deficiencies include smaller optical depths over North America relative to the midlatitude Pacific. ISCCP also shows an optical-depth maximum over the Tibetan plateau not evident in SKYHI. This may be a result of ISCCP's definition of cirrus in terms of
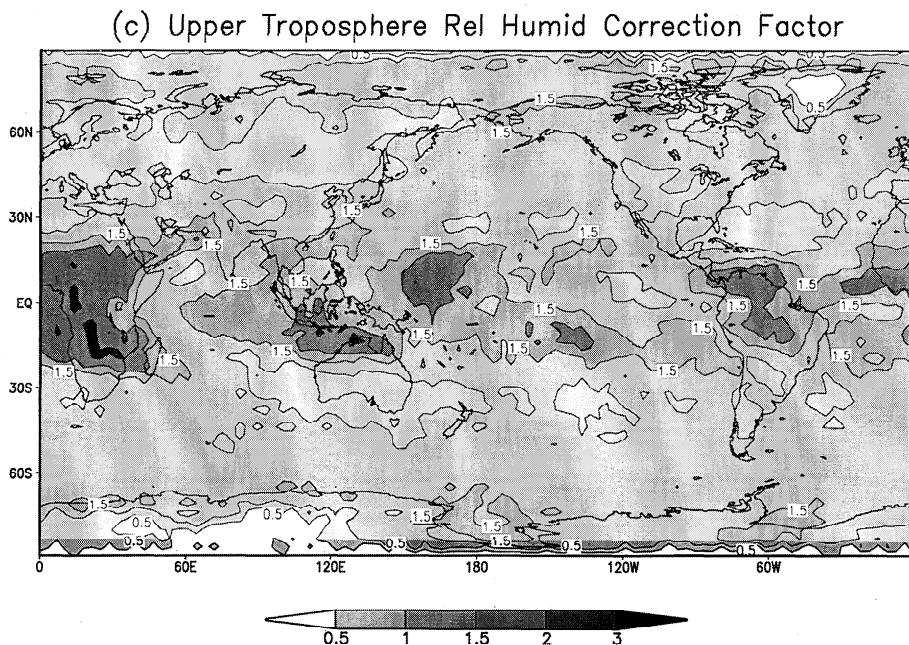
(c) Upper Troposphere Rel Humid Correction Factor

Figure 6. (continued)

pressures, which are sufficiently low over the Tibetan plateau that boundary layer clouds may be indicated as cirrus. There is a general tendency for tropical optical thicknesses to be higher in ISCCP than SKYHI. An obvious contributor to the low values in SKYHI is its low fractional areas relative to ISCCP (Figure 1). Numerous deficiencies in parameterization physics could also play roles, and the appendix considers specifically the possibility that subgrid variations in vertical velocity can produce systematic underestimates of optical depth, even in the absence of deficiencies in physical formulation. Plates 1d and 1e show the longwave emissivities for ice clouds for the "ice" and "bias-corrected" integrations. A striking aspect is the difference in the spatial distribution of emissivity relative to visible optical depth. This difference arises from the much stronger role of small effective crystal sizes in enhancing emissivity than visible optical depth in the microphysically dependent formulation of radiative properties of *Liou et al.* [1991]. (Note that the emissivities in Plates 1d and 1e are broadband and include the effects of in-cloud water vapor. They differ from narrowband emissivities which can be obtained from remote sensing and should be interpreted accordingly.) To provide some basis for comparison with field measurements of cloud properties, Plate 1f shows the time-mean visible optical depths, averaged conditionally upon cloud occurrence for the "bias-corrected" integration. The corresponding ISCCP fields are shown in Plate 1g. Note that the general tendency for smaller optical depths in SKYHI in Plates 1a and 1b is not evident in the conditionally averaged optical depths, especially in the tropics, where SKYHI optical depths are often larger than those of ISCCP. This result indicates that frequency of occurrence, rather than optical properties, explains some of the tropical discrepancy between SKYHI and ISCCP. However, the patterns of conditional optical depths in SKYHI and ISCCP still exhibit differences, with SKYHI's largest conditional optical depths in the tropics and ISCCP's largest conditional optical depths in the middle latitudes. Plate 1h shows the "bias-corrected" conditional emissivities. Note that even these large-scale ice clouds, which contain much less ice than anvil

cirrus associated directly with convection, can have fairly high emissivities in the conditional time mean.

Lin and Rossow [1996] inferred conditional ice paths in nonprecipitating clouds over oceans by combining ISCCP and microwave-imager data. Their estimates apply to anvil and mixed-phase clouds, in addition to the large-scale ice clouds treated here. To the extent that SKYHI and *Lin and Rossow* [1996] present realistic ice paths, the latter should be greater than the former, although the magnitude of the difference is difficult to assess a priori. For February 1988, *Lin and Rossow* [1996] report ice paths between 50°S and 30°N. Their conditional paths range from 20 to 100 g m^{-2} but show little systematic variation with latitude between about 20°S and 30°N, where they are mostly between 80 and 100 g m^{-2}. These values are greater than those shown in Figure 2c from SKYHI. Since SKYHI's bias-corrected conditional optical depths in much of the tropics are larger than ISCCP's (Plates 1f, 1g, and Figure 4), *Lin and Rossow*'s [1996] larger ice paths there could result from anvil and mixed-phase clouds, among such other factors as issues related to converting ice paths to optical depths (e.g., crystal sizes). ISCCP's conditional optical depths show much less variation with latitude than SKYHI's. SKYHI's conditional and unconditional (Plates 1a–1c and Figure 4) optical depths are lower than ISCCP's in middle latitudes. Low ice paths may be important at those latitudes, where SKYHI fractional areas are larger than ISCCP fractional areas. Large-scale, middle-latitude ice is often associated with synoptic fronts and jet streams, which can support variations in vertical velocity with scales below those resolved by SKYHI. As Appendix A shows, neglecting these subgrid velocity variations can lead to low parameterized ice paths.

In evaluating SKYHI and the ice-cloud parameterization, it is important to consider not only the mean fields but also the distributions of cloud events leading to the mean fields. Figure 5 presents distributions of conditional nonconvective cirrus by optical depth. Optical depths in Figure 5 range from 0.1 to 3.6. This range coincides with that adopted by ISCCP for cirrus, with the lower limit chosen to avoid ambiguities associated

(a) "Ice" LW Ice-Cloud Forcing [W/(m**2)]

(b) "Ice" SW Ice-Cloud Forcing [W/(m**2)]
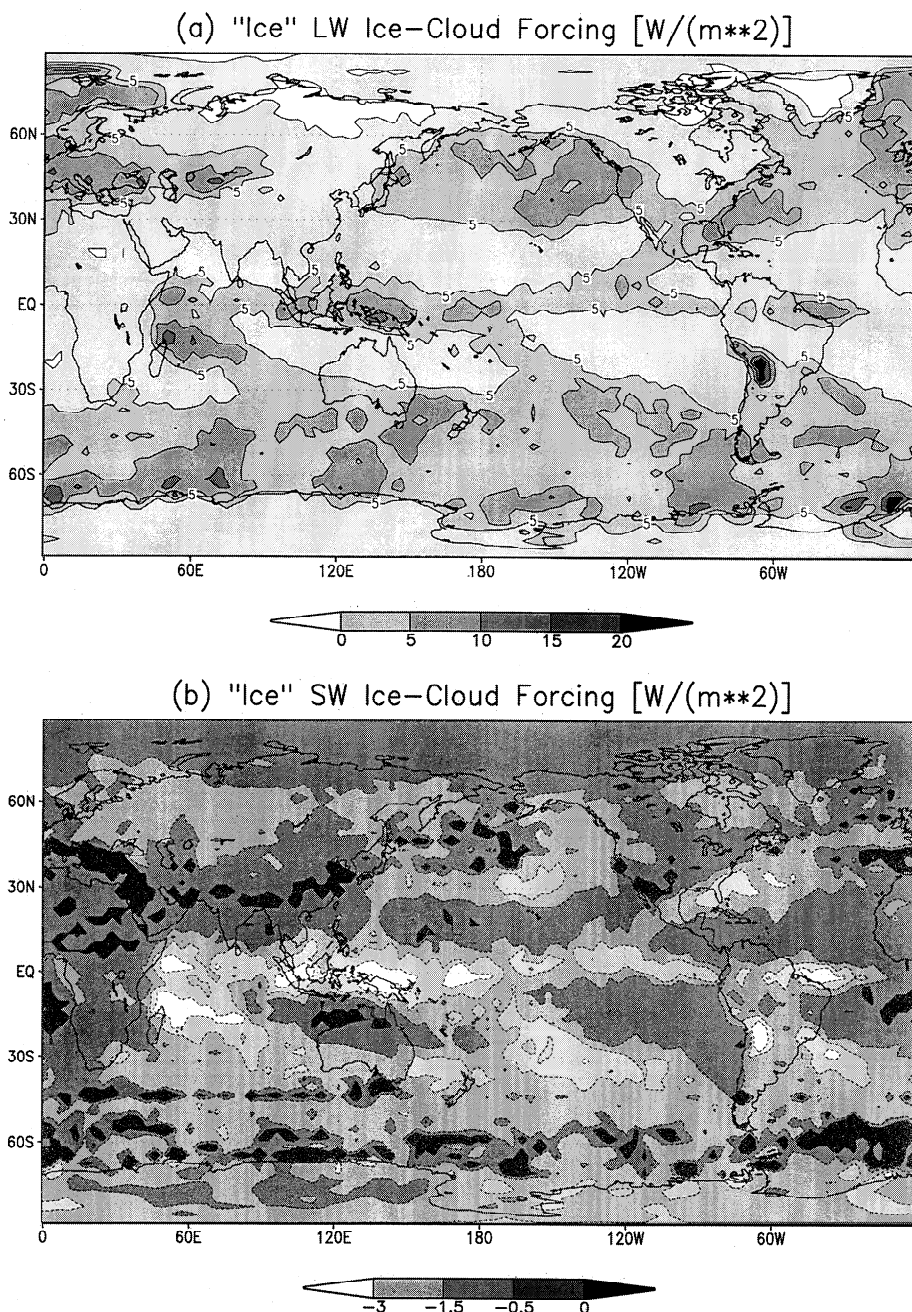
Figure 7. Top-of-atmosphere (a) longwave and (b) shortwave forcing by ice clouds ("ice" integration). Top-of-atmosphere total longwave cloud forcing for (c) "ice" integration, (d) "bias-corrected" integration, and (e) the Earth Radiation Budget Experiment (ERBE) January–March 1986–1989.

with detecting very thin cirrus. The "ice," "bias-corrected," and ISCCP distributions all peak at the lowest optical depths. Agreement between ISCCP and SKYHI is better for tropical clouds than those in the extratropics; ISCCP has more optically thicker clouds in the extratropics than SKYHI, as was also suggested by Plate 1g.

Figure 2 and Plate 1 show that the application of a bias correction produces significant improvements in the ice-cloud distributions over South America and Africa. These bias corrections are shown in Figure 6. Note that in the tropical upper troposphere, the bias correction produces higher temperatures, larger vertical velocities in the southern hemisphere, and higher relative humidities. The bias correction for relative hu-

midity is concentrated in several major regions and straightforwardly explains most of the regional ice-cloud changes in the tropics between the "ice" and the "bias-corrected" integrations. There is some offset of larger optical depths by a reduced frequency of occurrence in the "bias-corrected" integration (Figure 1); factors leading to the reduced frequency will be discussed subsequently.

4. Impact of Ice Clouds on Thermodynamics, Hydrology, and Dynamics

Figure 7 illustrates the top-of-atmosphere forcing by ice clouds. This forcing is defined as the radiative-flux difference
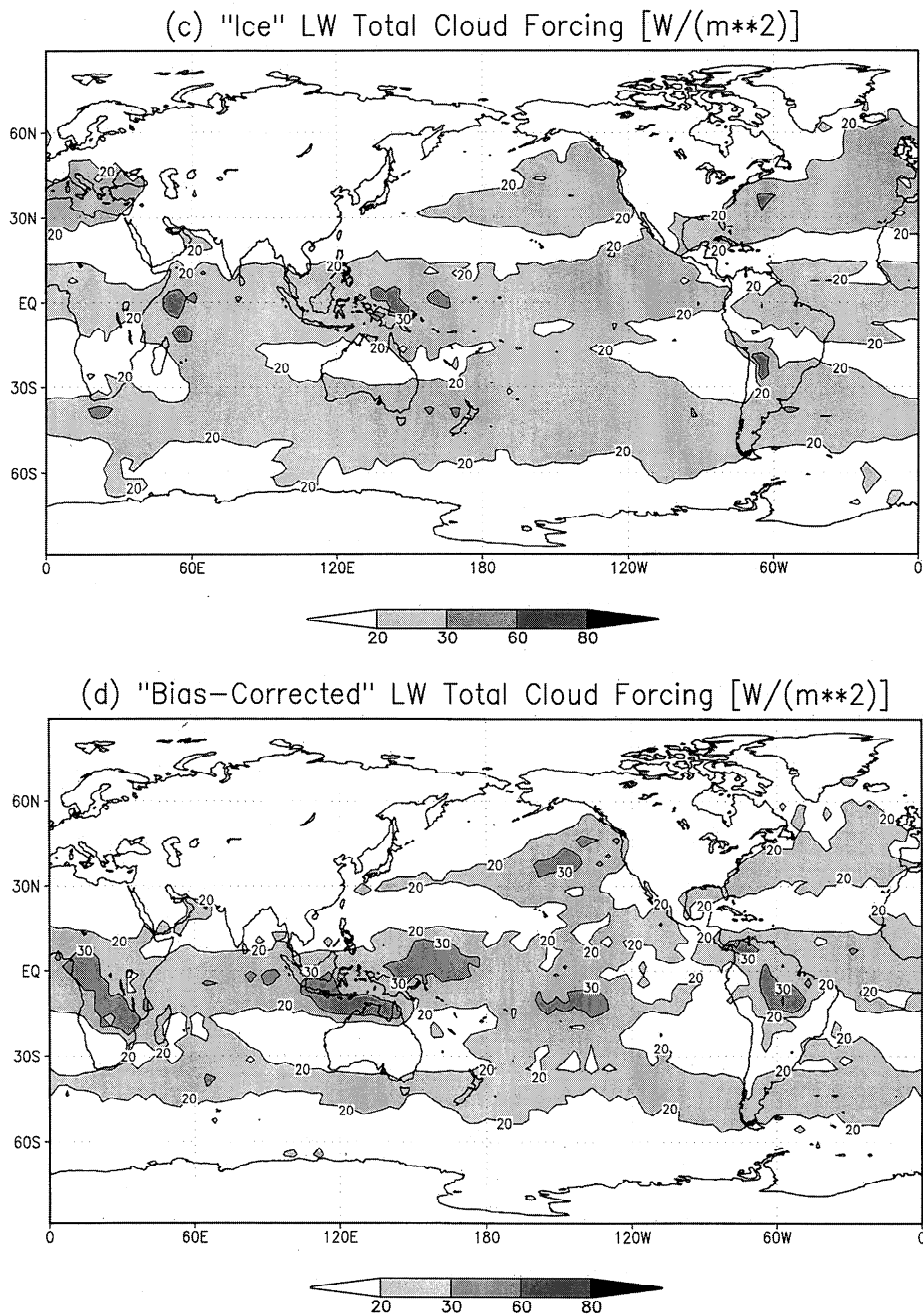
(c) "Ice" LW Total Cloud Forcing [W/(m**2)]

(d) "Bias-Corrected" LW Total Cloud Forcing [W/(m**2)]

Figure 7. (continued)

produced by ice clouds only; that is, liquid clouds do not contribute to the forcing, in contrast to the total cloud forcing often employed elsewhere. The ice-cloud forcing is calculated at every grid column and time by subtracting radiative fluxes obtained from the complete calculation from those obtained for identical columns except that the ice clouds only are removed. Note that the distributions of longwave and shortwave forcing differ significantly, with shortwave forcing concentrated in the tropics and longwave forcing significant in both the middle latitudes and the tropics. These differences are direct consequences of the differences in visible optical depths and longwave emissivities shown in Plate 1, which arise from the distributions of effective crystal sizes. This difference is a remarkable demonstration of the potential interactions between cloud microphysics, radiation, and large-scale climate

forcing. For ice clouds, heating by longwave forcing dominates cooling by shortwave forcing. It is important to note that interactions between deep convection, anvil microphysics, and anvil radiation have not been treated in detail; doing so would probably lead to more negative shortwave cloud forcing than shown in Figure 7.

The net, globally averaged forcing by large-scale ice clouds in Figure 7 is 4.8 W m^{-2}. The net imbalance between shortwave and longwave radiative fluxes at the top of the atmosphere in the "ice" integration is 4.3 W m^{-2} (upward), while it is 6.4 W m^{-2} (upward) in the "no ice" integration, with less trapping of longwave radiation in the latter case. Note that feedbacks reduce the net flux difference from ice clouds to 2.1 W m^{-2}; these feedbacks are not included in the radiative-forcing calculation, which holds all factors except for ice fixed.

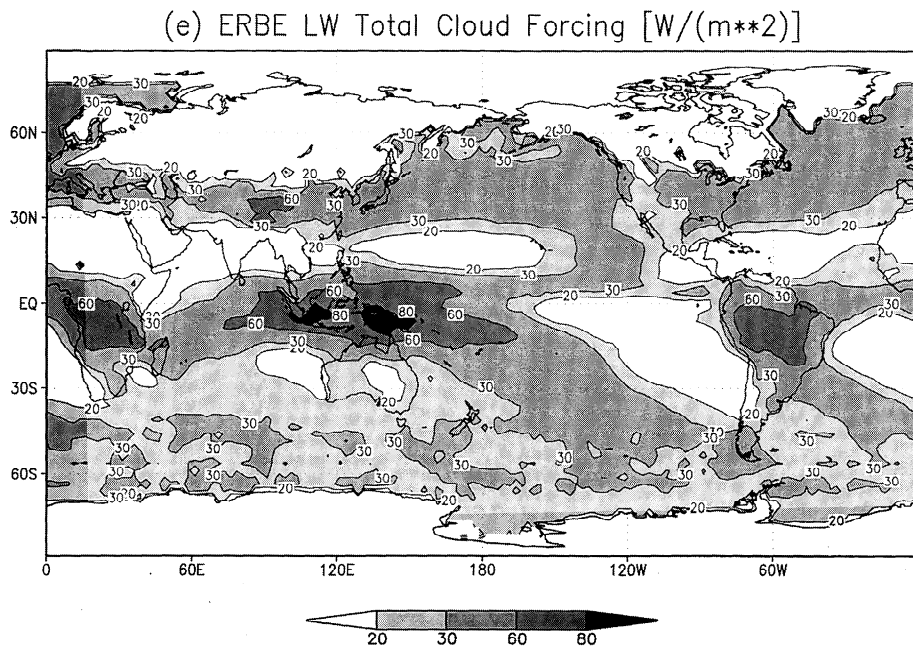## (e) ERBE LW Total Cloud Forcing [W/(m**2)]

Figure 7. (continued)

These results also demonstrate the sensitivity of top-of-atmosphere fluxes to the presence of ice clouds; for reference, the imbalance in the "control" version of SKYHI (with fixed clouds not removed at cold temperatures) is 6.4 W m^{-2} (downward), a result of emissivities of unity assigned to the fixed clouds, significantly reducing the upward emission of longwave radiation.

Comparisons with observations in section 3 focused mostly on visible properties of ice clouds from ISCCP. To compare longwave radiative properties of SKYHI ice clouds and observed clouds, total top-of-atmosphere longwave cloud forcings from SKYHI and the Earth Radiation Budget Experiment (ERBE) [e.g., *Harrison et al.*, 1990] (averaged for January–March 1986–1989) are presented in Figures 7c–7e. These results must be interpreted cautiously, since SKYHI's liquid clouds are prescribed and zonally symmetric. Upper tropospheric clouds contribute strongly to longwave cloud forcing, so total longwave cloud forcing provides some insight on the behavior of ice clouds, even though it does not isolate them as in Figures 7a and 7b. (Since SKYHI's total shortwave cloud forcing is determined largely by prescribed, zonally symmetric near-surface clouds, its shortwave forcing is mostly a pattern of zonally symmetric strips, which does not provide much information on upper tropospheric ice clouds.) SKYHI's longwave cloud forcing is generally less than ERBE's, consistent with lower visible optical depths in SKYHI, discussed in section 3. The bias correction increases the magnitude of cloud forcing in many regions, and cloud forcing is in better agreement with ERBE in the tropics, with distinct maxima over Africa, the western Pacific, and South America. The low tropical cloud fractional areas, noted on Figure 1, are likely major contributors to low longwave cloud forcing there.

The impact of ice clouds on SKYHI's zonally averaged temperature is shown in Figure 8a. In the "no ice" integration, fixed ("control") clouds are removed at temperatures below 258 K, as described in section 2.5, but no ice clouds are allowed to form. Statistically significant increases in temperature of up

to 3 K are noted in the tropical upper troposphere. (To calculate t statistics, each month of integration is taken as an independent event.) SKYHI is quite variable in the polar night around 100 to 200 hPa, and the larger temperature increases there are less significant and will not be further discussed. The temperature increases in Figure 8a are consistent with the net positive ice-cloud forcing (Figure 7). In the "ice" integration, ice forms over a broad range of pressures between 100 and 700 hPa (Figure 9b) in the tropics. The ice absorbs upwelling longwave radiation, again consistent with the pattern of warmer temperatures.

Figure 8b illustrates temperature differences between the "ice" integration and the "control" version of SKYHI, in which the fixed-cloud distribution is maintained for all clouds. The temperature increases in the upper tropical troposphere in Figure 8a are joined by significant temperature decreases of smaller magnitude in the middle tropical troposphere in Figure 8b. The temperature changes in Figures 8a and 8b differ because of differences in both the radiative properties and the vertical distributions of the fixed ice clouds in the "control" integration relative to those in the "ice" integration. Between 30°N and 30°S, conditional zonally averaged "ice" emissivities range from 0.25 to 0.42, while zonal (unconditional) averages range from 0.02 to 0.06, due to low fractional areas (Figure 1), much lower than the "control" conditional and zonal averages of unity and around 0.2, respectively. The fixed ice clouds in the "control" integration are restricted to a layer between roughly 240 and 300 hPa. The pattern in Figure 8b is a superposition of changes associated with removing the "control" ice clouds ("no ice" – "control") and then adding the "ice" clouds ("ice" – "no ice"). Tropical temperature changes for "no ice" – "control" (not shown) are dominated by reduced temperatures (2–4 K) between about 200 and 500 hPa. These reductions result from removal of the fixed ice clouds with consequent reduced absorption and trapping of longwave radiation. When clouds from the "ice" integration (Figure 8a) are superposed, upper tropospheric temperature increases above the

(a) Temperature Diff (K): "Ice" — "No Ice"

## (b) Temperature Diff (K): "Ice" — "Control"
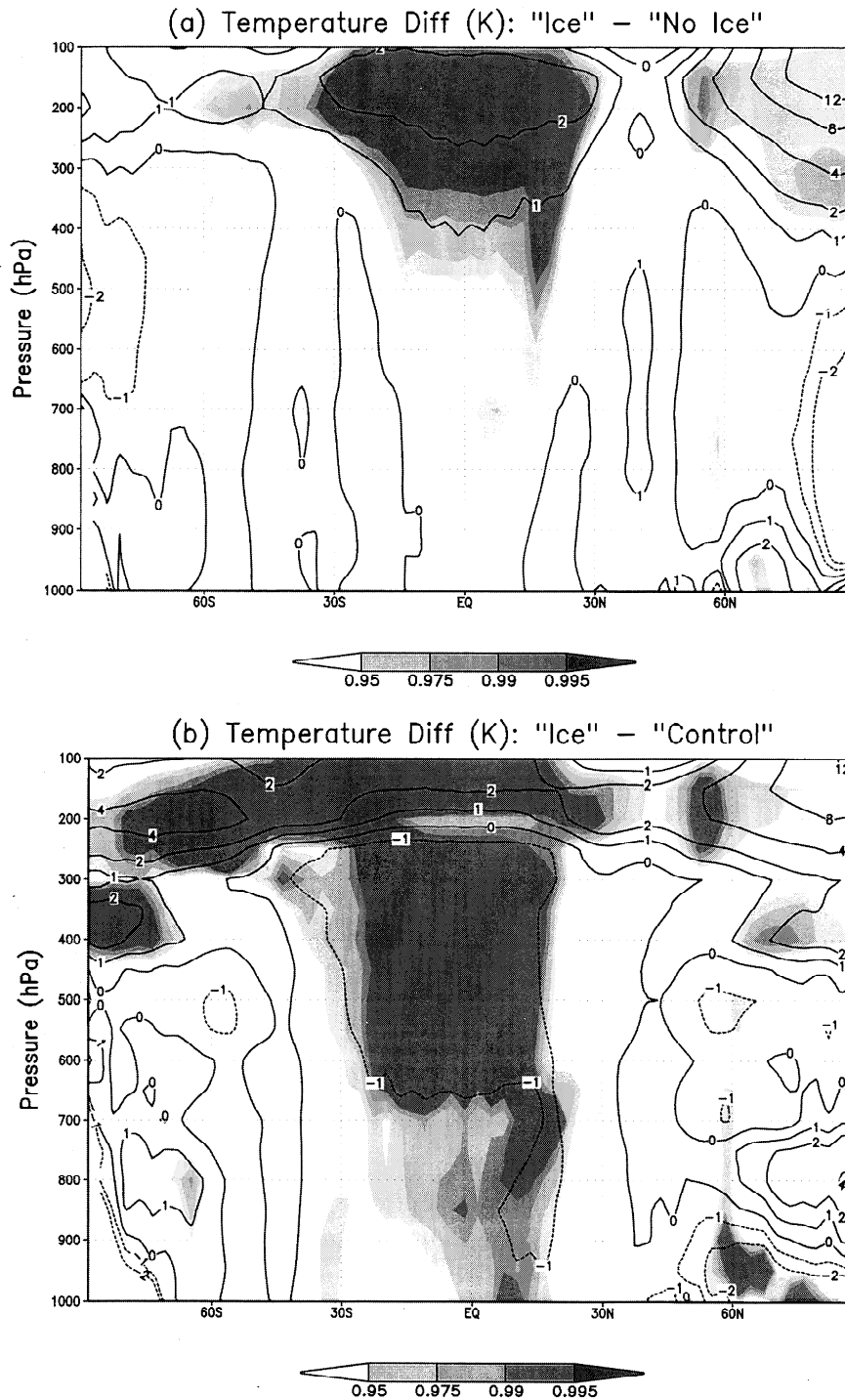
Figure 8. Zonally averaged temperature differences between (a) "ice" and "no ice" and (b) "ice" and "control" SKYHI integrations. Probabilities that differences are significant according to a t test are indicated by shading.

location of the "control" fixed clouds remain. Below the location of the "control" fixed clouds, temperature reductions associated with removing fixed clouds are larger in magnitude than temperature increases associated with adding "ice" clouds, but these increases lessen the temperature reductions. The changes associated with removing the "control" ice clouds are larger because their emissivities are larger. The presence of warmer upper tropospheric temperatures in Figures 8a and 8b,

despite opposing changes in emissivities, depends strongly on the different cloud vertical distributions in the two cases.

Although the t test used to assess the significance of temperature changes is intended for use with small samples (under 30 events or so), it assumes that differences are normally distributed. The small sample size in these integrations may raise concerns about the validity of this assumption. Nonparametric tests relax this assumption and can be used to assess differ-

(a) "Ice" Experiment — Radiative Heating (K/day)

(b) "Ice" Experiment — Large–Scale Ice (mg/kg)
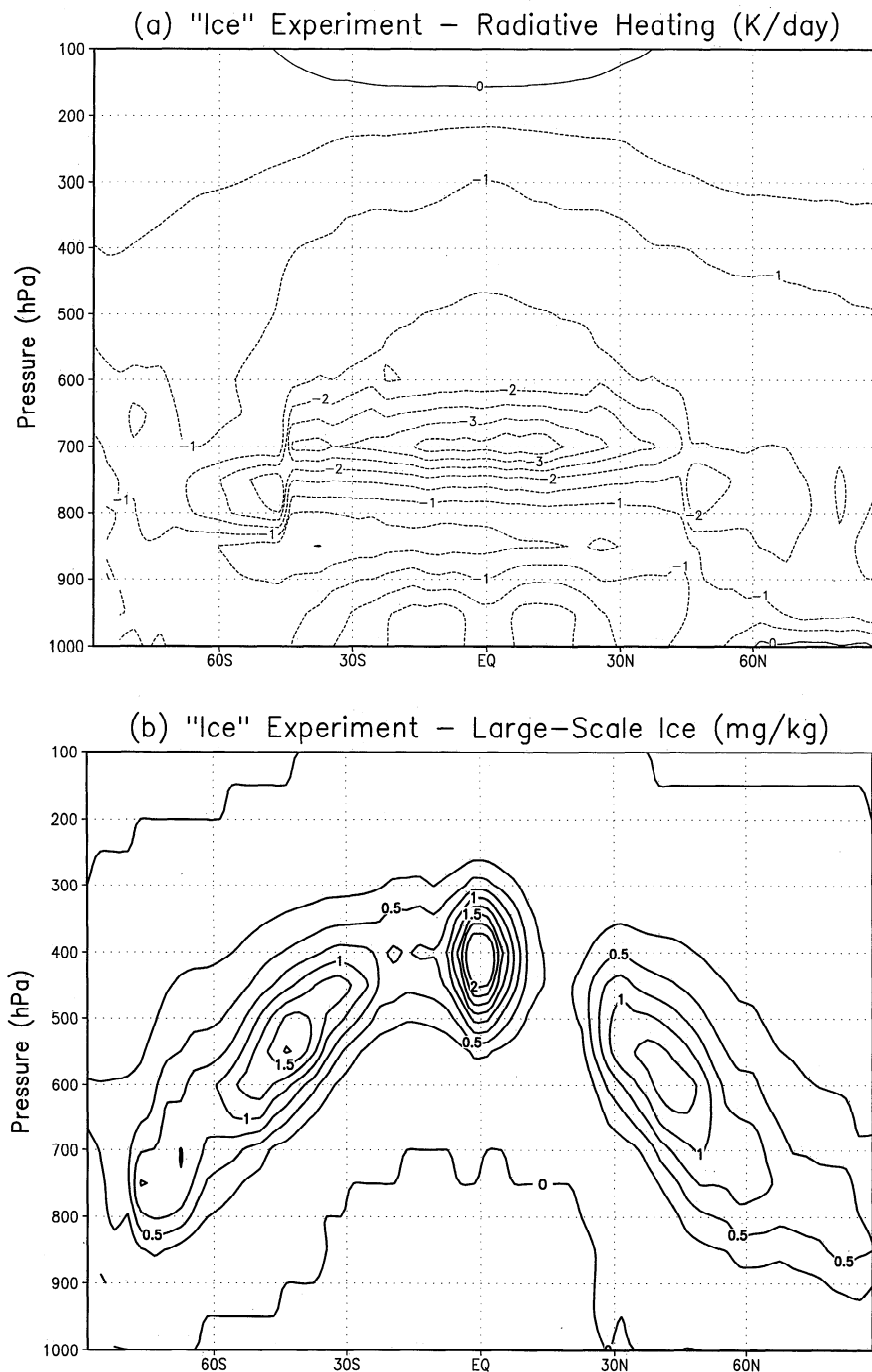
Figure 9. Zonally averaged (a) radiative heating and (b) ice mixing ratio for "ice" integration. (c) Zonally averaged radiative-heating differences between "ice" and "no ice" integrations. Contour intervals: (a) 0.5 K d^{-1}, (b) 0.25 mg kg^{-1}, (c) 0.1 K d^{-1}.

ences further [*Lanzante*, 1996]. The Wilcoxen signed-ranks test removes the assumption that differences are normally distributed, while retaining assumptions that they are continuous and symmetrically distributed. The binomial test removes even the assumption that differences are symmetrically distributed but uses only information on their signs (not magnitudes). The maximum confidence levels that can be attained with these methods are lower than those from the t test (e.g., 0.75 for the binomial test for the number of cases in Figure 8), but agreement among regions of maximum significance from these tests is useful in assessing the importance of difference features. All

difference features on Figure 8 with 0.99 t-test confidence have confidence levels of 0.75 with both the Wilcoxen and binomial tests.

Figure 9a shows the radiative-heating distribution for the "ice" integration. The largest cooling rates are in the middle tropical troposphere. Figure 9b shows the zonally averaged, time-mean distribution of ice. The differences in radiative heating between the distribution in Figure 9a and that associated with the "no ice" integration (Figure 9c) are consistent with the ice distribution. Radiative cooling is reduced beneath the ice for all three of the ice maxima shown in Figure 9b.
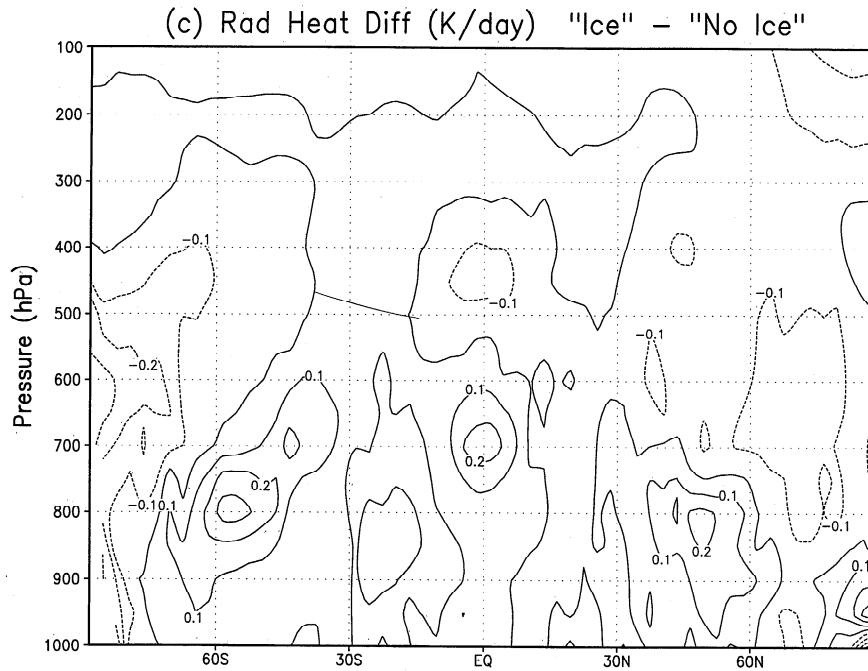
(c) Rad Heat Diff (K/day) "Ice" − "No Ice"

Figure 9.   (continued)

Radiative cooling is slightly increased in areas where ice is concentrated, consistent with enhanced emission of longwave radiation at cloud tops.

The ice clouds in SKYHI interact through phase changes with SKYHI's thermodynamic and hydrological cycles. Figure 10a shows the mixing-ratio tendency associated with the formation and dissipation of large-scale ice clouds. Water vapor is removed in the upper parts of the ice clouds, where deposition to ice occurs; water vapor is added in the lower parts of the ice clouds, where sublimation in unsaturated layers occurs. Large-scale ice clouds thereby vertically redistribute water vapor; very little of the ice reaches the Earth's surface. The changes in water-vapor mixing ratio produced by ice clouds are depicted in Figure 10b. Note that the pattern is not correlated with the direct moisture forcing produced by phase changes. Rather, they are related to large-scale dynamic responses to the ice. Figures 10c and 10d show the mean meridional streamfunction in the "ice" integration and the changes in it produced by the ice clouds. (The mean meridional streamfunction is defined as $2\pi a_e \cos \phi g^{-1} \int_P^{p_g}[v]\, dp'$, where ϕ, a_e, $[v]$, and p_g denote latitude, the Earth's radius, time-mean zonally averaged meridional velocity, and pressure at the Earth's surface, respectively.) Note that the ice clouds act to increase the intensity of the Hadley circulation; its maximum streamfunction magnitude increases by approximately 14%. *Slingo and Slingo* [1988] and *Randall et al.* [1989] found that forcing associated with all clouds also increased the intensity of the Hadley circulation, and *Lohmann and Roeckner* [1995] found that the Hadley circulation intensified as cirrus emissivity increased. The stronger upward motions at the equator transport more water vapor into the tropical troposphere; enhanced subsidence at the poleward branches of the Hadley cell leads to decreased mixing ratios there. The increased intensity of the Hadley cell and the associated changes in the water-vapor distribution can be related to the changes in diabatic heating associated with the

ice clouds. Figure 9c shows they reduce radiative cooling with a local maximum in the reduction in the lower tropical troposphere, centered at the equator at 700 hPa. The effect of this pattern of reduced cooling is to increase the equatorward gradient of the total diabatic heating. The intensity of the Hadley circulation increases with the equatorward diabatic-heating gradient generally [cf. *Holton*, 1992, chapter 10]; the changes in radiative cooling and the zonally symmetric circulation associated with large-scale ice clouds follow such a pattern. The larger rates of ascent in the Hadley circulation in "ice" in turn lead to increased heating from convective adjustment, strengthening further the diabatic-heating gradient and providing a positive feedback on the dynamic effect of the ice itself. Thus changes in SKYHI's hydrological cycle are produced by ice clouds, not directly through their associated phase changes but indirectly through their effect on diabatic-heating gradients and planetary-scale circulations.

Further consideration of the "bias-corrected" integration provides another example of the delicate balances between microphysical and radiative properties. As a result of positive temperature corrections (Figure 6a), ice paths increase when clouds form, as can be seen in Figure 2c, which shows ice paths, conditionally averaged on ice-cloud occurrence, for the "ice" and "bias-corrected" integrations. The optically thicker clouds (Figure 4) in the "bias-corrected" integration absorb more longwave radiation and reflect more solar radiation back into the overlying atmosphere. In the tropical upper troposphere, temperatures are warmer ($\sim$2–4 K) in "bias corrected" than in "ice," and ice is displaced upward in the "bias-corrected" integration (Figure 11a). At the altitudes where most tropical ice clouds form, temperatures increase but water-vapor mixing ratios do not, resulting in lower relative humidities (Figure 11b). Since ice formation depends on a threshold relative humidity, the frequency of occurrence of ice clouds decreases

(a) Moisture Forcing by Large-Scale Ice (g/kg/day)

(b) Water-Vapor Mixing-Ratio Diff (g/kg) "Ice" − "No Ice
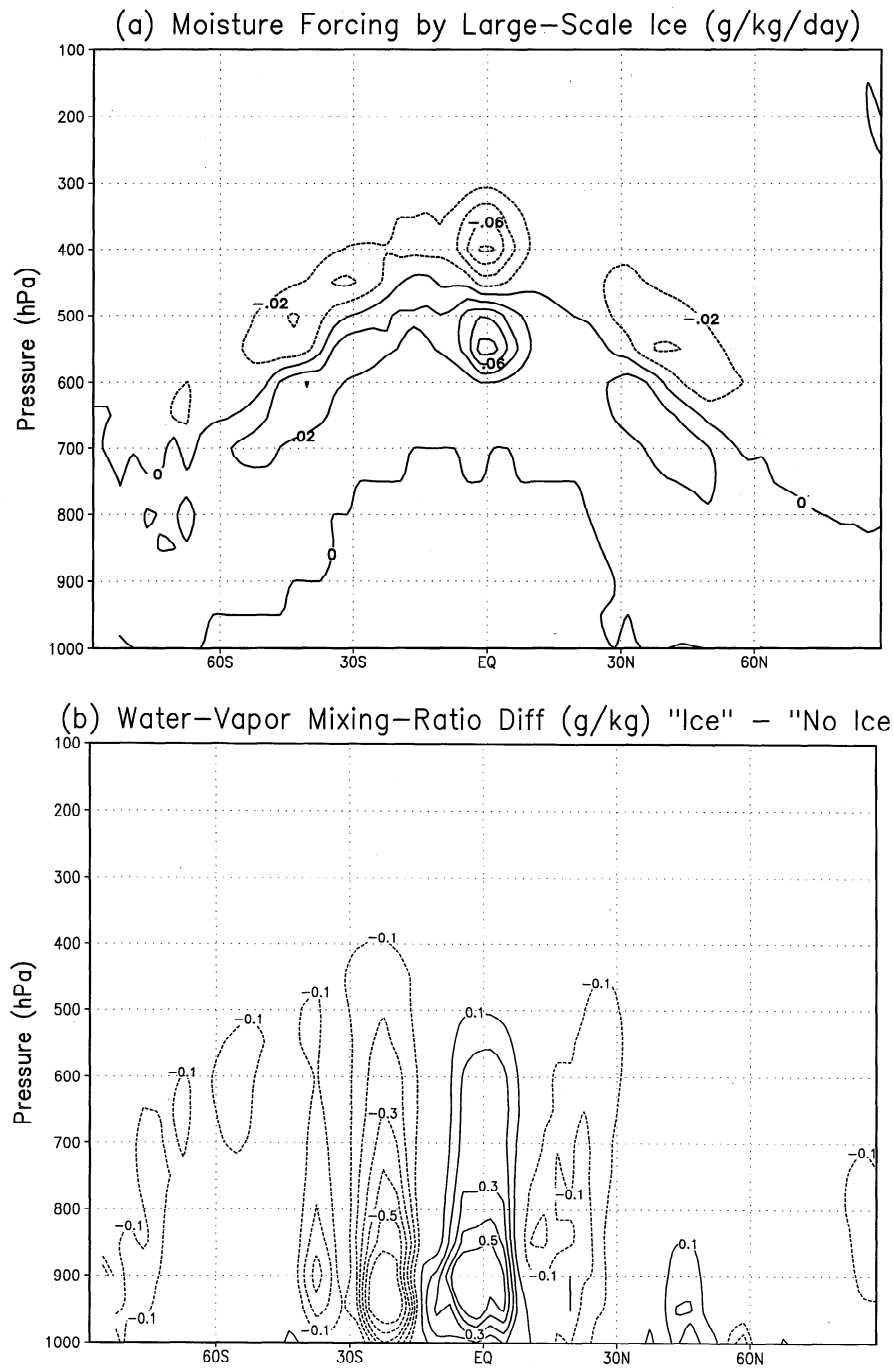
Figure 10. (a) Zonally averaged moisture forcing by large-scale ice; (b) zonally averaged water-vapor mixing-ratio differences between "ice" and "no ice" integrations; (c) meridional stream function for "ice" integration; (d) stream function differences between "ice" and "no ice" integrations. Contour intervals: (a) 0.02 g kg^{-1} d^{-1}, (b) 0.1 g kg^{-1}, (d) 10^{12} kg s^{-1}.

(Figure 1), a negative feedback on the higher conditional ice concentrations produced by applying the bias correction. The lower frequency of occurrence in the "bias-corrected" integration results in (unconditional) zonally averaged ice paths that are similar for the "ice" and "bias-corrected" integrations in the tropics and lower for the "bias corrected" than the "ice" integration in middle and high latitudes. A further adjustment of the threshold relative humidity for the "bias-corrected" integration could offset this negative feedback to some extent.

5. Impact of Ice Clouds on Climate Sensitivity

The sensitivity of a general circulation model (GCM) climate can be measured by examining the ratio of global- and time-mean temperature change at the Earth's surface to the associated change in the net radiative flux at the top of the atmosphere [Cess et al., 1989]. A sensitivity analysis of this type for SKYHI's "ice" and "no ice" integrations is presented in Appendix B. Note that cloud forcing in this section refers to
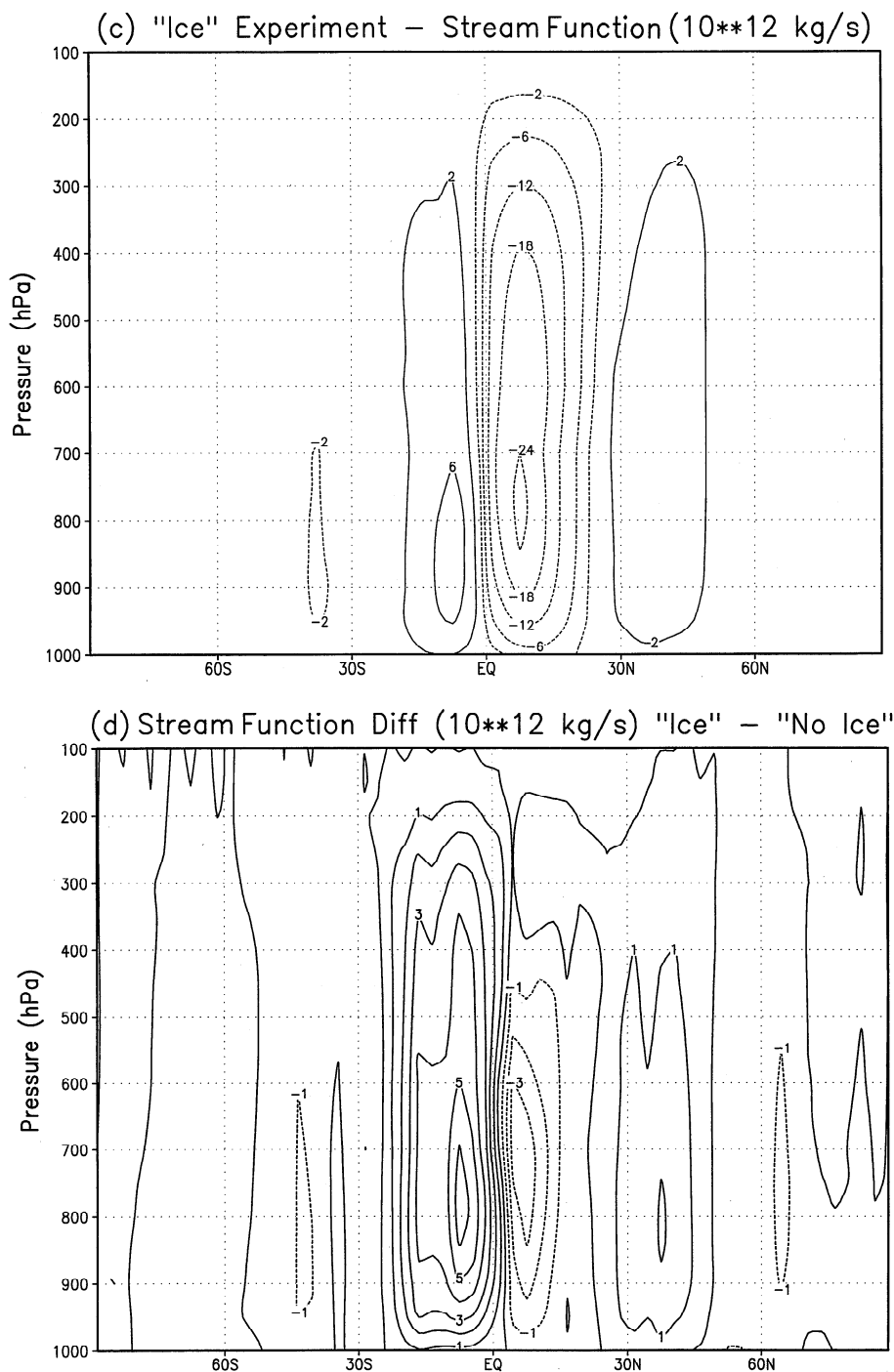
Figure 10. (continued)

the total cloud forcing by both ice and liquid clouds. It is important to note that the prescribed distributions of liquid clouds in both integrations render SKYHI quite insensitive; the closest GCM in the work of Cess et al. [1989] has a climate sensitivity of 0.39 K $(W\,m^{-2})^{-1}$. The change in radiative flux at the top of the atmosphere in this sensitivity analysis is produced by differencing SKYHI integrations in which sea surface temperatures (SST) have been uniformly perturbed by +2 K and −2 K from the appropriate control integration.

Appendix B shows that SKYHI's sensitivity increases only slightly due to ice clouds, a result that is not surprising given that liquid clouds are largely fixed and exert a strong restraint on flux changes to the Earth-atmosphere system. Some changes in the distribution of liquid clouds do occur, however; these changes are a result of temperature changes across the threshold of 258 K, below which liquid clouds do not exist. The components of the sensitivity change in Appendix B can be largely interpreted from these changes in liquid clouds and ice-cloud changes. As atmospheric temperatures increase with SST, more liquid clouds form. These additional liquid clouds act to reduce the increased longwave emission associated with higher SSTs. In the "ice" integration the offsetting effect of increased liquid clouds is diminished by the presence of ice clouds, leading to a larger increase in emitted longwave flux
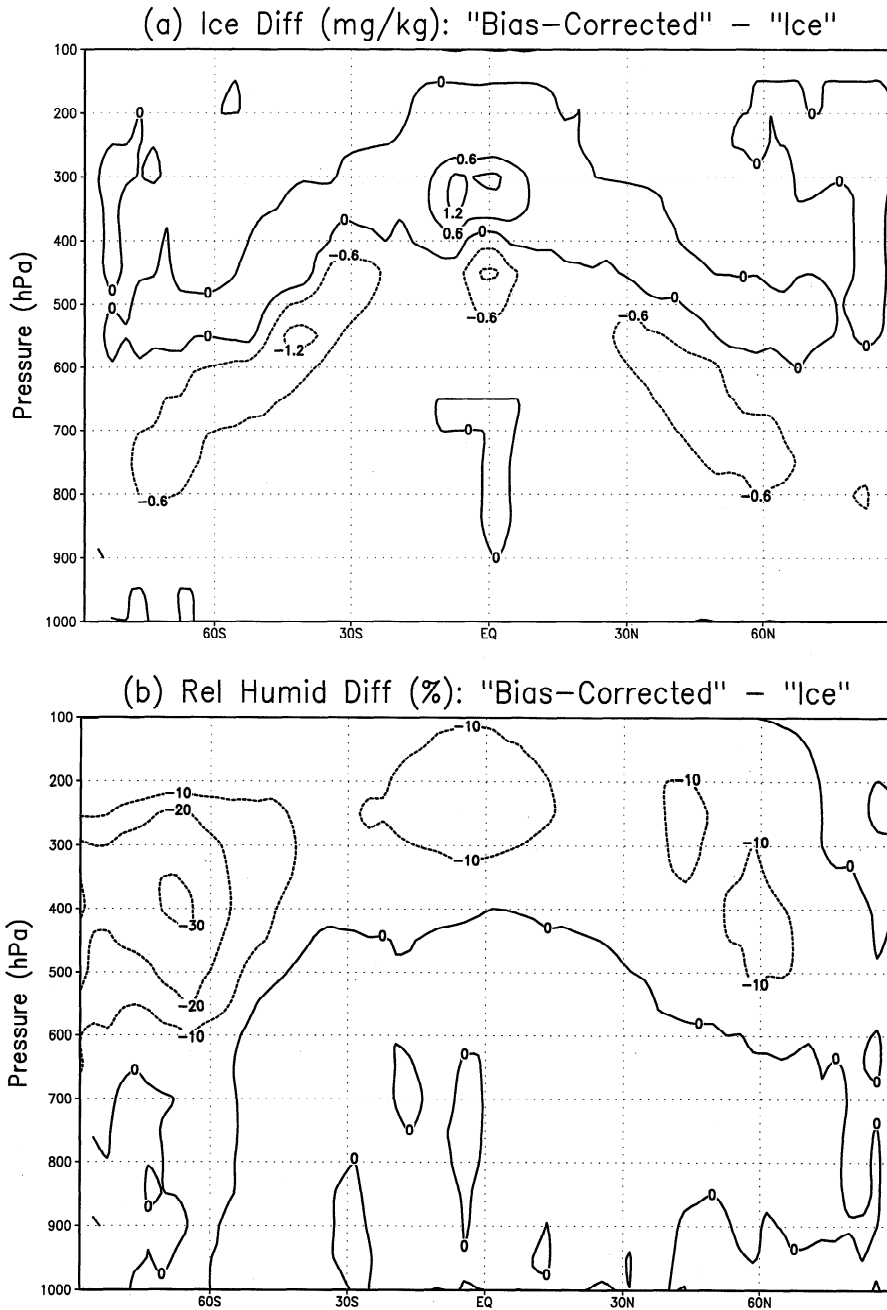
Figure 11. (a) Zonally averaged ice-mixing-ratio difference between "bias-corrected" and "ice" integrations; (b) zonally averaged relative humidity difference between "bias-corrected" and "ice" integrations. Contour intervals: (a) 0.6 mg kg^{-1}, (b) 10%.

ΔF. Ice clouds are present in both the low and the high SST integrations in "ice." The chief difference between the cases is that they are located at higher altitudes with high SST. Longwave trapping is thus present in both the low and the high SST cases in "ice," and the impact on ΔF is less than in "no ice," where the liquid clouds represent a relatively larger perturbation. This difference between "ice" and "no ice" is also evident in the smaller value of Δ (longwave cloud forcing) in "ice." The effect of ice clouds is especially pronounced where atmospheric temperatures increase above the 258 K threshold as SST increases. In those cases, areas with no clouds change to areas with liquid clouds in "no ice," while areas which may contain ice clouds (depending on vertical velocity, etc.) change

to areas with liquid clouds in "ice." The change is smaller in "ice," consistent with the smaller change in longwave cloud forcing. The change in the altitude of the ice clouds with SST has a negligible effect on the shortwave cloud forcing. Therefore the change in downward solar flux ΔQ differs between "no ice" and "ice" mostly due to changes in clear-sky radiation. Its smaller magnitude in "ice" is associated with larger tropical water-vapor mixing ratios (compare Figure 10b). Water-vapor mixing-ratio variations lead to larger clear climate sensitivities than complete climate sensitivities. The smaller value of Δ (longwave cloud forcing) in "ice" leads to a larger decrease in net cloud radiative forcing in "ice," which is a larger fraction of the net change in upward flux G at the top of the atmosphere.

The analysis of climate sensitivity in this version of SKYHI reveals a rather complex set of interactions involving ice clouds, liquid clouds, and water vapor. Climate sensitivity could behave very differently with other parameterizations for liquid clouds, mixed-phase clouds, and anvil clouds.

6. Summary

Large-scale, nonconvective ice clouds in the SKYHI GCM, parameterized as a balance between ice formation by deposition from vapor and ice removal by settling and sublimation, broadly resemble those observed by satellites. During the northern hemisphere winter, key ice areas are located over the western tropical Pacific, Indian Ocean, North Pacific, parts of North America, Europe, and the North Atlantic. With corrections for mean biases, ice also forms over tropical Africa and South America. Regional variations in both ice-water path and mean effective particle size are important in determining the radiative properties of ice clouds. The longwave emissivities of the clouds respond much more strongly to particle size than the visible optical depths, leading to major differences in the patterns of the most intense longwave and shortwave forcing by ice clouds. In general, ice clouds heat the Earth-atmosphere system. Their major effect on zonally averaged temperatures is to increase them in the upper tropical troposphere. The diabatic heating associated with ice clouds increases the intensity of SKYHI's Hadley circulation, leading to larger water-vapor mixing ratios.

Ice clouds in SKYHI agree reasonably with limited observations despite important parameterization simplifications. Of particular concern is the use of a threshold relative humidity to determine whether clouds exist. Although the threshold used here is based on a comparison of frequencies of occurrence of relative humidity and ISCCP ice clouds, the comparison used globally averaged data. Cirrus fractional areas in SKYHI (determined by the threshold humidity) are less than ISCCP areas in the tropics and greater than ISCCP areas at middle and high latitudes (Figure 1), demonstrating that a global threshold is limited, at least with SKYHI's distribution of humidity biases (Figure 6c). A related issue, not considered in this paper, is fractional area for ice clouds; large-scale ice clouds have been assumed to have fractional area of unity, although the parameterization can easily be used with smaller fractional areas. Radiative properties of ice clouds have been shown to depend on ice-crystal sizes, yet their treatment at GCM scales is difficult and has followed an empirical approach here. The parameterization solves for equilibrium ice concentrations and does not include horizontal advection of ice, in addition to ignoring subgrid horizontal variability (Appendix A). Of course, the parameterization adopts highly simplified microphysics (deposition, sublimation, melting, and sedimentation only).

Nonconvective ice clouds comprise an important component of the climate system. Convective ice and liquid clouds are treated very simply in this study; radiative and dynamic interactions are likely to increase significantly when these components are treated more consistently with the nonconvective ice.

Appendix A: Impact of Subgrid Variability on Ice Content

Plates 1f and 1g show that conditionally averaged optical depths in some regions are lower in SKYHI than ISCCP. Many observational and parameterization uncertainties could be re-

sponsible, although by conditional averaging the direct effect of parameterizing frequency of occurrence is eliminated. Several areas of lower SKYHI optical depths, for example, off the east coasts of Asia and North America and in the Southern Ocean southwest of Australia, are near jet streams at altitudes where ice clouds form frequently. This appendix demonstrates that subgrid variations in flow properties which drive the ice parameterization (e.g., vertical velocity) are a possible explanation for lower parameterized ice contents. The strong horizontal wind shears near jets in the regions noted above can generate large amounts of subsynoptic variability (turbulence and gravity waves), and these regions are especially likely to be subject to this subgrid effect.

The formation of ice in saturated areas requires ascent in this parameterization. Therefore vertical velocity is an especially strong control and will be used as an example of subgrid-scale effects on large-scale parameterized ice concentrations. A set of large-scale vertical velocities $\langle w \rangle$ typical of regions with cirrus formation was constructed. A corresponding set of parameterized ice contents $X[\langle T \rangle, \langle w \rangle]$, based only on grid-scale vertical velocities, like those calculated in SKYHI, was also constructed. In contrast, ice contents can be calculated for each large-scale case by using a set of subgrid vertical velocities

$$w = \langle w \rangle + \delta r(-0.5, 0.5), \qquad (A1)$$

where δ is the amplitude of the subgrid variation, and $r(-0.5, 0.5)$ is a randomly generated number between -0.5 and 0.5. The ice contents $\langle X(T, w) \rangle$ include the effects of subgrid variations in vertical velocities, having been averaged horizontally after application of the nonlinear parameterization.

To estimate δ for midlatitude synoptic systems, aircraft measurements of w over various length scales, taken near Munich on March 18, 1994, were used (Figure A1). The observed standard deviations at the shortest length scales can be used to estimate δ. By comparing $X[\langle T \rangle, \langle w \rangle]$, which represents a GCM application of the parameterization ignoring subgrid variations, with $\langle X(T, w) \rangle$, the effect of subgrid variation in w is evident. Figure A2 shows this effect can be quite large; ice contents calculated without subgrid variations are generally below those with variations by factors of two or more.
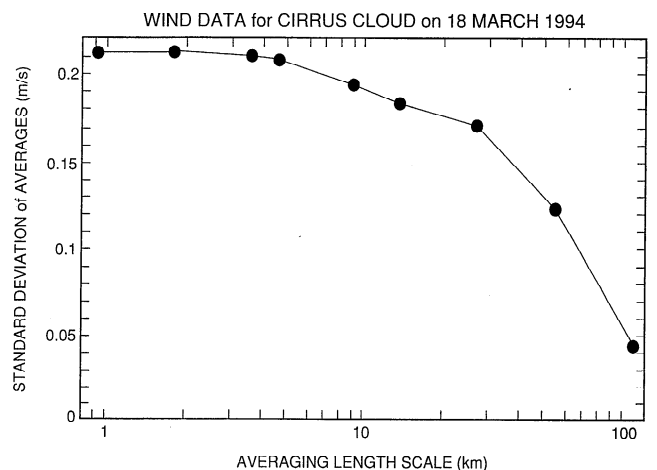
Figure A1. Standard deviations of vertical velocity as function of length scale over which velocity averaged. Aircraft data were taken near Munich on March 18, 1994.
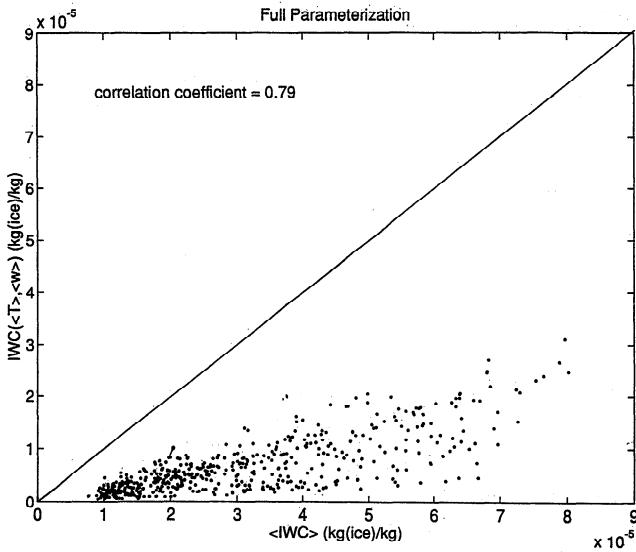
Figure A2. Ice mixing ratios calculated using grid averages of vertical velocity IWC ($\langle T \rangle$, $\langle w \rangle$) versus mixing ratios averaged from calculations of ice content at subgrid scales $\langle$IWC$\rangle$.

Subgrid variations in nonlinear parameterizations may generally be associated with results such as these. Serious deficiencies in parameterized properties are possible, even with a correct parameterization. Consideration should be given to subgrid variations in parameterization drivers when applying such parameterizations at scales larger than the scales for which the parameterizations are physically valid. Analogous problems characterize the calculation of grid-average radiative transfer in the presence of subgrid variations in microphysical properties [*Tiedtke*, 1996]; a complete representation of subgrid effects would require parameterizing these effects on both microphysics and radiation.

Appendix B: Impact of Ice Clouds on Climate Sensitivity

$$G = \Delta F - \Delta Q \qquad (B1)$$

F is global-mean emitted TOA longwave flux; Q is global-mean downward TOA solar flux; and ΔT_s is change in global-mean surface temperature.

Climate sensitivity

$$\lambda = \Delta T_s / G \qquad (B2)$$

$$\Delta\text{CRF} = \Delta(\text{longwave cloud forcing})$$

$$+ \Delta(\text{shortwave cloud forcing}) \qquad (B3)$$

$$\text{Longwave cloud forcing} = F_{\text{clear}} - F \qquad (B4)$$

$$\text{Shortwave cloud forcing} = Q - Q_{\text{clear}} \qquad (B5)$$

Clear climate sensitivity

$$\lambda_{\text{clear}} = \frac{\lambda G}{\Delta\text{CRF} + G} \qquad (B6)$$

Δ is ("control" SST + 2 K) − ("control" SST − 2 K).

No Ice Clouds	Ice Clouds
$\lambda = 0.35$ K (W m^2)$^{-1}$	$\lambda = 0.36$ K (W m^2)$^{-1}$
$\Delta F = 8.9$ W m^{-2}	$\Delta F = 9.6$ W m^{-2}
$\Delta Q = -2.7$ W m^{-2}	$\Delta Q = -2.2$ W m^{-2}
$\Delta T_s = 4.1$ K	$\Delta T_s = 4.2$ K
Δ(longwave cloud forcing) = 0.74 W m^{-2}	Δ(longwave cloud forcing) = 0.33 W m^{-2}
Δ(shortwave cloud forcing) = −4.0 W m^{-2}	Δ(shortwave cloud forcing) = −4.0 W m^{-2}
ΔCRF = −3.3 W m^{-2}	ΔCRF = −3.7 W m^{-2}
ΔCRF/G = −0.28	ΔCRF/G = −0.31
$\lambda_{\text{clear}} = 0.49$ K (W m^2)$^{-1}$	$\lambda_{\text{clear}} = 0.52$ K (W m^2)$^{-1}$
$\lambda/\lambda_{\text{clear}} = 0.72$	$\lambda/\lambda_{\text{clear}} = 0.69$

Notation

a visible albedo, dimensionless.
a_e radius of Earth, m.
C_i constant for albedo calculation, dimensionless.
D width of an ice crystal, m.
D_e mean effective size for ice-particle distribution, m.
g gravity constant, m s^{-2}.
F ice flux, kg (ice) m^{-2} s^{-1}.
L maximum dimension of an ice crystal, m.
$n(L)$ density function for ice-particle size distribution, m^{-3} m^{-1}.
p pressure, Pa.
p_g pressure at Earth's surface, Pa.
r randomly generated number, dimensionless.
r_e effective radius for ice-particle distribution, m.
t time, s.
T temperature, K.
v meridional velocity, m s^{-1}.
V_t mean ice terminal speed, m s^{-1}.
X_s ice mass mixing ratio, kg kg^{-1}.
X_v water-vapor mixing ratio, kg kg^{-1}.
w vertical velocity, m s^{-1}.
α constant in optical-depth formula, m^2 kg^{-1}.
β constant in optical-depth formula, m m^2 kg^{-1}.
δ subgrid vertical-velocity amplitude, m s^{-1}.
ρ air density, kg m^{-3}.
τ optical depth, dimensionless.
ϕ latitude, deg.
ζ cosine of zenith angle, dimensionless.
Δp cloud pressure thickness, Pa.

The following apply generally:

$\overline{(\ )}$ vertical average over the thickness of a cloud.
$\langle(\ )\rangle$ grid-scale average.
$(\ )_{\text{max}}$ maximum limit.
$(\ )_{\text{min}}$ minimum limit.
$(\ )_{\text{sat}}$ bottom layer of an ice-saturated cloud.
$(\ )_{\text{sub}}$ bottom of a sublimating ice cloud.
$[(\ )]$ time-mean zonal average.

Additional symbols are defined in Appendix B.

ISCCP data were supplied by the NASA Langley DAAC. A core code for processing SKYHI fields was provided by R. John Wilson.

References

Cess, R. D., et al., Interpretation of cloud-climate feedback as produced by 14 atmospheric general circulation models, *Science, 245,* 513–516, 1989.

Ebert, E. E., and J. A. Curry, A parameterization of ice cloud optical properties for climate models, *J. Geophys. Res., 97,* 3831–3836, 1992.

Fels, S. B., J. D. Mahlman, M. D. Schwarzkopf, and R. W. Sinclair, Stratospheric sensitivity to perturbations in ozone and carbon dioxide: Radiative and dynamical response, *J. Atmos. Sci., 37,* 2265–2297, 1980.

Hamilton, K., R. J. Wilson, J. D. Mahlman, and L. J. Umscheid, Climatology of the SKYHI troposphere-stratosphere-mesosphere general circulation model, *J. Atmos. Sci., 52,* 5–43, 1995.

Harrison, E. F., P. Minnis, B. R. Barkstrom, V. Ramanathan, R. D. Cess, and G. G. Gibson, Seasonal variation of cloud radiative forcing derived from the Earth Radiation Budget Experiment, *J. Geophys. Res., 95,* 18,687–18,703, 1990.

Heymsfield, A. J., and L. J. Donner, A scheme for parameterizing ice-cloud water content in general circulation models, *J. Atmos. Sci., 47,* 1865–1877, 1990.

Heymsfield, A. J., and C. M. R. Platt, A parameterization of the particle size spectrum of ice clouds in terms of the ambient temperature and the ice water content, *J. Atmos. Sci., 41,* 846–855, 1984.

Holton, J. R., *An Introduction to Dynamic Meteorology,* 511 pp., Academic, San Diego, Calif., 1992.

Jin, Y., W. B. Rossow, and D. P. Wylie, Comparison of the climatologies of high-level clouds from HIRS and ISCCP, *J. Clim., 9,* 2850–2879, 1996.

Lanzante, J. R., Resistant, robust, and non-parametric techniques for the analysis of climate data: Trends and examples, including applications to historical radiosonde station data, *Int. J. Climatol., 16,* 1197–1226, 1996.

Lin, B., and W. B. Rossow, Seasonal variation of liquid and ice water path in nonprecipitating clouds over oceans, *J. Clim., 9,* 2890–2902, 1996.

Liou, K. N., J. L. Lee, S. C. Ou, Q. Fu, and Y. Takano, Ice cloud microphysics, radiative transfer, and large-scale cloud processes, *Meteorol. Atmos. Phys., 46,* 41–50, 1991.

Lohmann, U., and E. Roeckner, Influence of cirrus cloud radiative forcing on climate and climate sensitivity in a general circulation model, *J. Geophys. Res., 100,* 16,305–16,323, 1995.

Mitchell, J. F. B., C. A. Senior, and W. J. Ingram, CO_2 and climate: A missing feedback?, *Nature, 341,* 132–134, 1989.

Ou, S. C., and K. N. Liou, Ice microphysics and climatic temperature feedback, *Atmos. Res., 35,* 127–138, 1995.

Ramanathan, V., and W. Collins, Thermodynamic regulation of ocean warming by cirrus clouds deduced from the 1987 El Nino, *Nature, 351,* 27–32, 1991.

Ramanathan, V., E. J. Pitcher, R. C. Malone, and M. L. Blackmon, The response of a spectral general circulation model to refinements in radiative processes, *J. Atmos. Sci., 40,* 605–630, 1983.

Randall, D. A., Harshvardan, D. A. Dazlich, and T. G. Corsetti, Interactions among radiation, convection, and large-scale dynamics in a general circulation model, *J. Atmos. Sci., 46,* 1943–1970, 1989.

Rossow, W. B., A. W. Walker, D. E. Beuschel, and M. D. Roiter, International Satellite Cloud Climatology Project (ISCCP): Implementation of new cloud datasets, *WMO Tech. Data, WMO/TD-737,* 115 pp., World Clim. Res. Programme, World Meteorol. Organ., Geneva, 1996.

Senior, C. A., and J. F. B. Mitchell, Carbon dioxide and climate: The impact of cloud parameterization, *J. Clim., 6,* 393–418, 1993.

Slingo, J. M., The development and verification of a cloud prediction scheme for the ECMWF model, *Q. J. R. Meteorol. Soc., 113,* 899–927, 1987.

Slingo, A., and J. M. Slingo, The response of a general circulation model to cloud longwave radiative forcing, I, Introduction and initial experiments, *Q. J. R. Meteorol. Soc., 114,* 1027–1062, 1988.

Soden, B. J., and F. P. Bretherton, Upper tropospheric relative humidity from the GOES 6.7 μm channel: Method and climatology for July 1987, *J. Geophys. Res., 98,* 16,669–16,688, 1993.

Starr, D. O'C., and D. P. Wylie, The 27–28 October 1986 FIRE cirrus case study: Meteorology and clouds, *Mon. Weather Rev., 118,* 2259–2287, 1990.

Tiedtke, M., An extension of cloud-radiation parameterization in the ECMWF model: The representation of subgrid-scale variations of optical depth, *Mon. Weather Rev., 124,* 745–750, 1996.

Wallace, J. M., Effect of deep convection on the regulation of tropical sea surface temperature, *Nature, 357,* 230–231, 1992.

Warren, S. G., Atlas of simultaneous occurrence of different cloud types over land, *NCAR Tech. Note, NCAR/TN-241+STR,* 214 pp., Natl. Cent. for Atmos. Res., Boulder, Colo., 1986.

Warren, S. G., C. J. Hahn, J. London, R. M. Chervin, and R. L. Jenne, Atlas of simultaneous occurrence of different cloud types over land, *NCAR Tech. Note, NCAR/TN-241+STR,* 214 pp., Natl. Cent. for Atmos. Res., Boulder, Colo., 1984.

Warren, S. G., C. J. Hahn, and J. London, Simultaneous occurrence of different cloud types, *J. Clim. Appl. Meteorol., 24,* 658–667, 1985.

Warren, S. G., C. J. Hahn, J. London, R. M. Chervin, and R. L. Chervin, Global distribution of total cloud cover and cloud type amounts over the ocean, *NCAR Tech. Note, NCAR/TN-317+STR,* 212 pp., Natl. Cent. for Atmos. Res., Boulder, Colo., 1988.

Wetherald, R. T., and S. Manabe, Cloud feedback processes in a general circulation model, *J. Atmos. Sci., 45,* 1397–1415, 1988.

L. J. Donner, R. S. Hemler, C. J. Seman, B. J. Soden, and J. C. Warren, NOAA Geophysical Fluid Dynamics Laboratory, Princeton University, P.O. Box 308, Princeton, N. J. 08542. (e-mail: ljd@gfdl.gov)

K.-N. Liou, Department of Meteorology, University of Utah, Salt Lake City, UT 84112.

J. Ström, International Meteorological Institute, University of Stockholm, Stockholm, Sweden.